

On Controlling the Kinematics of a Filament Stretching Rheometer Using a
Real-Time Active Control Mechanism [†]

Submitted to *Journal of Non-Newtonian Fluid Mechanics*, January 15, 1999

Shelley L. Anna

*Division of Engineering and Applied Sciences, Harvard University
Cambridge, MA 02138 U.S.A.*

Chris Rogers

*Department of Mechanical Engineering, Tufts University
Medford, MA 02174 U.S.A.*

Gareth H. McKinley

*Department of Mechanical Engineering, Massachusetts Institute of Technology
Cambridge, MA 02139 U.S.A.*

[†] This paper was presented at the *Mechanics of Nonlinear Materials* conference, Banff, Canada, May 1998.

Abstract

We present two new experimental methods of realizing the desired kinematics in a filament stretching rheometer. Due to the presence of the rigid plates connecting the fluid filament in this device, a homogeneous uniaxial elongational flow cannot be imposed throughout the entire fluid filament. However, if the fluid element at the midpoint of the filament is forced to contract in the same manner as a cylindrical column undergoing ideal uniaxial extension, then the measured rheological response will be virtually identical to that experienced in a homogeneous shearfree flow. We investigate both a real-time active control scheme and a second, original technique based on a one-dimensional slender-filament approximation of the kinematics as possible methods of realizing this form of nearly-ideal filament stretching experiment.

We find that the real-time active control scheme induces undesirable oscillations in the imposed plate separation profile, leading to unacceptable fluctuations in the measured force data and limiting the achievable operating range of the device. The second technique, on the other hand, produces very accurate and smooth mid-point diameter profiles in a two-step process. Transient Trouton ratio data obtained by using the second method with both a polystyrene-based Boger fluid and a polyisobutylene-based Boger fluid agree well with data previously reported in the literature. Differences between the transient Trouton ratios at intermediate strains obtained from experiments in which the midpoint diameter decreases either ideally or inhomogeneously are consistent with expectations from recent simulations. The second technique presented here provides a simple method of achieving accurate filament stretching data that can be compared quantitatively with theoretical constitutive models.

Keywords: Extensional rheometry, filament stretching rheometer, Transient extensional viscosity, Trouton ratio, Boger fluid, polystyrene, polyisobutylene.

1. Introduction

Understanding the extensional behavior of polymeric fluids has been of long-standing interest since the kinematics of the deformation lead to a very different dynamical response in the fluid microstructure than that observed in a simple shearing flow. However, a basic understanding of the extensional behavior of many non-Newtonian fluids, especially the more ‘mobile’ dilute polymer solutions, has been difficult to achieve [1]. Numerous devices, including the opposed jet rheometer, two- and four-roll mills, the converging channel rheometer, and many more, have been used to try to characterize extensional behavior of these mobile fluids [2,3]. The filament stretching device has recently emerged as one of the most controllable and accurate methods of measuring the extensional viscosity of a fluid.

The filament stretching device was pioneered early in this decade by Matta and Tytus [4], and was further developed by Sridhar and coworkers over the next few years [5,6]. Several groups around the world, including Spiegelberg *et al.* [7,8], Kröger, Berg *et al.* [9,10], Solomon and Muller [11], Koelling *et al.* [12], Van Nieuwkoop and Muller Von Czernicki [13], and Verhoef *et al.* [14] have subsequently constructed filament stretching devices of various designs. In addition, several groups have begun to investigate the details of the flow in the filament stretching device via numerical simulations, using various constitutive models [15 - 21].

In order to probe the extensional behavior of a fluid, one desires to impose a flow that effectively isolates extensional kinematics from any shearing deformation that arises from inhomogeneities induced by the experimental device. In homogeneous pure uniaxial elongation, a cylindrical fluid sample is uniformly stretched in such a way that local fluid elements move apart exponentially in time. The filament stretching device attempts to create such a purely elongational flow by placing a small sample of fluid

between two circular endplates and moving these rigid fixtures apart so that the gap between the plates increases exponentially in time. However, an additional shearing component of flow is induced near the endplates due to the no-slip boundary condition. This non-ideality in the flow has been investigated experimentally by Spiegelberg and McKinley [7] and numerically by Kolte *et al.* [16] and Yao and McKinley [18]. The stability of the motion has recently been examined by Olagunju [19]. For small strains, the flow closely approximates a ‘reverse’ squeeze flow that can be accurately represented by a lubrication analysis. At larger strains for Deborah numbers greater than $De > 0.5$ the experimental and numerical investigations all show that the deformation in the central portion of the filament becomes increasingly homogeneous. Kolte *et al.* discuss three types of experiments that can be performed in the filament stretching device, each of which result in very different deformation history within the elongating fluid column. Comparison of these three experimental protocols demonstrates that it is possible, at least in theory, to impose a flow in the filament stretching device that minimizes the effect of non-idealities, and leads to transient stress growth in the fluid which is nearly identical to the stress growth in a purely elongational flow.

The focus of this paper is not to measure the transient extensional viscosity of a particular fluid, *per se*, but rather to realize the three types of experiments discussed in [16], using a new filament stretching device with an extended operating space. The resulting insights and kinematic analysis should then be of broad use in the systematic design and optimization of the operation of any filament stretching device. The desired kinematics in the fluid filament are achieved via two different techniques, the first involving real-time active (‘closed-loop’) control of the mid-filament diameter as a function of time. The second technique is a much simpler, essentially ‘open-loop’, technique based on a one-dimensional approximation of the fluid response in the filament stretching device. To demonstrate the performance of these differing control protocols,

we measure the transient extensional rheology of two different constant-viscosity, ideal-elastic Boger fluids, both of which have been previously investigated by Spiegelberg *et al.* [7,8]. Results for transient extensional viscosities obtained using the new methods are shown to match previous results at intermediate Hencky strains, and the data are also extended to higher final strains than previously measured, allowing the evolution of stress growth toward a steady state plateau to be monitored. The principal benefit of the new control techniques presented here is that they eliminate much of the tedious iterative design of endplate velocity profiles that has accompanied filament stretching rheometry to date.

In Section 2, we briefly review the relevant features of the slender filament approximation and introduce definitions and notation for the three different experiments we will discuss. In Section 3, we describe the specifics of the filament stretching device used in this paper and the formulations and viscometric properties of the fluids tested. In Sections 4 and 5 we describe the concept and application of the active control scheme and the 1-D formulation scheme, respectively, and in Section 6 we present the results of applying these two schemes on two different PS- and PIB-based Boger fluids. Finally, Section 7 summarizes the main points discussed in this paper.

2. Background

2.1. Slender Filament Approximation

Before commencing filament stretching experiments, it is helpful to make a simple prediction as to how a fluid filament will deform given a particular set of imposed boundary conditions. Figure 1 shows a sketch of a filament stretching apparatus, and defines the coordinate system and boundary conditions we use in mathematical analyses of the experiment. A one-dimensional model for the filament can be constructed by first recognizing that there are typically two widely disparate length scales in the fluid

filament, i.e. the rapidly increasing endplate separation $L_p(t)$, and the rapidly shrinking mid-filament diameter $D_{mid}(t)$. Consequently, over most of the filament, the derivative $\partial D(z,t)/\partial z$ is small and the axial component of the curvature is negligible for aspect ratios $\Lambda(t) = L_p(t)/(D_{mid}(t)/2) \gg 1$. This so-called ‘‘slender filament approximation’’ leads to the assumption that the axial velocity, \mathbf{v}_z , in the filament depends only on the axial position and time. More detailed derivation of the resulting one-dimensional equations of motion in Lagrangian and Eulerian coordinates are given by Renardy [22] and Eggers [23] respectively. A general one-dimensional formulation of the velocity field satisfying continuity can be written as

$$\begin{aligned} \mathbf{v}_z(z,t) &= F(z,t) \\ \mathbf{v}_r(r,z,t) &= -\frac{1}{2}r \frac{\partial F}{\partial z} \end{aligned} \quad (1)$$

with boundary conditions given by

$$\begin{aligned} z = -L_p(t)/2: \quad \mathbf{v}_z &= 0 \\ z = +L_p(t)/2: \quad \mathbf{v}_z &= \dot{L}_p(t) \equiv \dot{E}(t)L_p(t) \end{aligned} \quad (2)$$

A complete formulation requires the appropriate stress boundary condition at the free surface, which is given by

$$\frac{\partial}{\partial z} \left[D^2(z,t)(\tau_{zz} - \tau_{rr})/4 + \sigma D(z,t)/2 \right] = 0 \quad (3)$$

where $D(z,t)$ denotes the diameter profile of the free surface, σ is the surface tension, and $(\tau_{zz} - \tau_{rr})$ is the tensile stress difference in a fluid element on the free surface [22]. Within the one-dimensional slender filament approximation, the no-slip boundary condition at $z = \pm L_p(t)$ cannot, in general, be satisfied and the approximation fails close to the rigid endplates [23]. The precise form of the function $F(z,t)$ depends on the initial profile of the filament $D(z,t=0)$, the externally imposed displacement $L_p(t)$, and the constitutive response of the elongating fluid column. In what follows, we assume that inertial effects in the viscous fluid filament are negligible. We will always use $\dot{E}(t)$ to represent the *imposed* or axial elongation rate; $\dot{\epsilon}_{eff}(t, z = L_p/2)$ to denote the effective

deformation rate for the Lagrangian element at the midplane of the elongating fluid column (computed from measurements of the midpoint diameter); and $\dot{\epsilon}_0$ to denote the ideal case in which the deformation rate experienced by this fluid element is temporally homogeneous.

One solution to the slender filament equations for an initially cylindrical sample leads to an Eulerian velocity field in which the axial velocity is *linear* in axial position, or, equivalently, a Lagrangian profile in which the plate separation increases *exponentially* in time. This condition on \mathbf{v}_z then leads to an exponentially decreasing filament diameter.

$$\mathbf{v}_z = \dot{\epsilon}_0 z \Rightarrow L_p(t) = L_0 e^{\dot{\epsilon}_0 t} \Rightarrow D(t) = D_0 e^{-\frac{1}{2}\dot{\epsilon}_0 t} \quad (4)$$

In general, other solutions to the slender filament equations must be computed numerically. It is worth noting that another solution of identical kinematic form to (1) is the lubrication solution for a Newtonian fluid confined between two rigid plates of aspect ratio $\Lambda_0 = L_0/(D_0/2) \ll 1$ [7]. In this limit, the appropriate conditions to satisfy are no slip and no flux at the endplates, since the effects of the free surface are confined to a radial region of order $L(t) \ll D(t)$ near the outer edge of the disks. The axial velocity in this case is a *cubic* function of the axial position,

$$\mathbf{v}_z = \dot{L}_p(t) \left[\frac{3}{2} \left(\frac{z}{L_p} \right) - 2 \left(\frac{z}{L_p} \right)^3 \right] \quad (5)$$

and the resulting deformation rate $\dot{\epsilon}(z,t)$ in the fluid is both spatially and temporally inhomogeneous. Consequently, an initially cylindrical fluid sample becomes concave at later times. However, if an exponentially increasing endplate separation is imposed, $L_p(t) = L_0 \exp(+\dot{E}t)$, the mid-filament diameter will still decrease exponentially, with an effective deformation rate, based on the actual evolution of the mid-filament diameter, that is 50 percent faster than the imposed elongation rate. Evaluating the radial velocity

at $z = 0$, $r = D_{mid}(t)/2$ leads to

$$D_{mid}(t) = D_0 e^{-\frac{3}{4}\dot{\epsilon}t} \quad (6)$$

and hence, the effective deformation rate is given by

$$\dot{\epsilon}_{eff} \equiv -\frac{2}{D_{mid}} \frac{dD_{mid}}{dt} = +\frac{3}{2}\dot{\epsilon}. \quad (7)$$

The solution to the general one-dimensional formulation for a viscoelastic material is expected to be significantly more complex than either of the two previous solutions; however, detailed comparisons with finite element calculations show that a one-dimensional formulation can still accurately capture the evolution in the fluid column during stretching (Harlen [24]) and also during stress relaxation and breakup (Yao and McKinley [18]). At early times, when $\Lambda(t) \ll 1$, the viscous response of the material dominates and the mid-filament diameter may be expected to follow the Newtonian lubrication response. At larger strains ($\Lambda(t) \gg 1$), the nonlinear viscoelastic nature of the fluid begins to play a role, and the evolution of the diameter profile can then reveal information about the constitutive behavior of the fluid. A complete solution is not possible unless the appropriate constitutive relationship for the fluid is known, and it is this relationship that is probed in a filament stretching experiment. However, the fact that the filament kinematics at all strains are of the form in equation (1) suggests the basis for a control strategy for filament stretching rheometers which we will explore in §3.

2.2. *Definitions of Material Functions for Transient Extensional Rheology*

In a uniaxial stretching flow, the desired material function is the transient extensional viscosity as a function of time and commanded elongation rate, $\dot{\epsilon}_0$. This transient extensional viscosity is defined in terms of the tensile stress growth in the fluid and the imposed deformation rate, according to the expression

$$\bar{\eta}^+(t, \dot{\epsilon}_0) = \frac{[\tau_{zz}(t) - \tau_{rr}(t)]}{\dot{\epsilon}_0}. \quad (8)$$

By performing a force balance on the filament, the transient extensional viscosity can be related to measured quantities, including the total force exerted on the endplate, $F_p(t)$ (corrected for surface tension and gravitational body forces), and the mid-filament diameter, $D_{mid}(t)$, which are shown schematically in Figure 1 [17]. The transient extensional viscosity is frequently expressed in non-dimensional form as the Trouton ratio, or the ratio of the transient extensional viscosity to the zero-shear-rate viscosity of the fluid, η_0 . Thus, the transient Trouton ratio is related to measured quantities by

$$Tr \equiv \frac{\bar{\eta}^+(t, \dot{\epsilon}_0)}{\eta_0} = \frac{[\tau_{zz}(t) - \tau_{rr}(t)]}{\eta_0 \dot{\epsilon}_0} = \frac{F_p}{\pi(D_{mid}/2)^2 \eta_0 \dot{\epsilon}_0}. \quad (9)$$

Three characteristic types of experiments that can be performed in the filament stretching device were first considered numerically by Kolte *et al.* [16]. These experiments differ in the precise form of the imposed endplate separation profile, and thus also exhibit different measured force and mid-filament diameter profiles. The first two experiments involve moving the endplates apart such that the plate separation increases at an exponential rate and the axial elongation rate is constant, $\dot{E}(t) = \dot{\epsilon}_0$. In a *Type I* experiment, the mid-filament diameter is *assumed* to follow an ideal profile such that $D_{ideal}(t) = D_0 \exp(-0.5\dot{\epsilon}_0 t)$. In reality, the diameter profile will not deform ideally due to the no-slip condition at the endplates (§2.1). Thus, in a *Type II* experiment, the measured, non-ideal mid-filament diameter is used to compute the temporally inhomogeneous *effective deformation rate* $\dot{\epsilon}_{eff}$ experienced by fluid elements near the midplane. The resulting Trouton ratio incorporates these non-ideal quantities, and is now computed via

$$Tr^{(II)} = \frac{F_p(t)}{\pi(D_{mid}(t)/2)^2 \eta_0 \dot{\epsilon}_{eff}(t)}. \quad (10)$$

The *effective Hencky strain* in the fluid element at the centerline can be determined directly from

$$\varepsilon_{eff}(0, t) = - \int_{\tilde{t}=0}^t \frac{2}{D_{mid}} \frac{dD_{mid}}{d\tilde{t}} d\tilde{t} = 2 \ln[D_0/D_{mid}]. \quad (11)$$

A more detailed description of these experiments is given by Kolte *et al.*, who compare numerical calculations for each type of experiment with results for an ideally deforming cylinder [16]. Kolte *et al.* show that results from a Type I experiment are the least accurate compared to those for an ideal deformation, but that incorporating the true mid-filament diameter profile in a Type II experiment significantly increases the accuracy. However, Kolte *et al.* find that yet another type of experiment is still more accurate, and in fact yields results that are indistinguishable from those for an ideally deforming cylinder. It is clearly desirable for experimentalists to perform *Type III* experiments in order to allow detailed comparisons with numerical models of ideal uniaxial flow.

The Type III experiment requires the mid-filament diameter to follow an ideal exponential deformation, given in equation (4), such that $\dot{\varepsilon}_{eff}(t) = \dot{\varepsilon}_0$. In other words, the fluid elements near the midplane now experience a *constant* stretch rate. To achieve this constraint, the velocity of the endplates, $\dot{L}_p(t)$, no longer follows the profile predicted by ideal uniaxial elongational flow, and thus the axial stretch rate, $\dot{E}(t)$, is no longer constant, in contrast to the Type I and Type II experiments. As Kolte *et al.* note in their paper, “this type of experiment is quite difficult to perform in practise...[requiring] either a very fast control mechanism for the plate motion based on inline observations of the mid-filament diameter or a trial-and-error procedure...” [16]. To date, all Type III experiments have used the latter, iterative method [5-14]. It is the goal of the current paper to show that not only can the active control alternative work, but that there is also a much simpler method of obtaining the ideal diameter profile using the simple one-dimensional kinematics of the filament stretching problem discussed in §2.1.

3. Experiment Procedure

3.1. Filament Stretching Device

Figure 2 shows a schematic diagram of the new filament stretching device used in this study. The apparatus is based around a motion control system consisting of two linear DC brushless motors moving along the same axis. The upper endplate assembly is mounted to the upper motor, and the lower endplate is mounted to a sensitive force transducer. This assembly is mounted to a rigid base that is mechanically uncoupled from the motor assembly. The lower motor platen carries a CCD laser micrometer that is used to measure the mid-filament diameter. In the experiments performed here, the top endplate/motor platen assembly moves away from the fixed bottom endplate according to a velocity profile specified by the user. The bottom motor platen moves in the same direction as the top motor, but at half the speed, in order that the diameter measurement is taken at the midpoint of the filament throughout the entire experiment.

The linear motors that control the endplate separation are manufactured by Northern Magnetics, Inc., controlled by a Delta Tau PMAC-Lite Controller, and powered by two Glentek three-phase amplifiers. The position of each motor can be controlled to within $\pm 150 \mu\text{m}$, and measured to within $\pm 1 \mu\text{m}$. The maximum total travel of the motors is $L_{\text{max}} = 180 \text{ cm}$, and the maximum speed is $\dot{L}_{\text{max}} = 300 \text{ cm/s}$. Position profiles can either be downloaded to the PMAC controller prior to the experiment, or they can be computed autonomously during an experiment.

The operating space of a filament stretching rheometer can be conveniently represented by plotting the velocity of the plates against the plate separation. Since the plate separation and the velocity in a filament stretching experiment nominally grow exponentially in time, an homogeneous stretching experiment can be represented as a

straight line on this operating diagram. The new filament stretching rheometer used in the current study has an extended operating space, shown in Figure 3, capable of achieving Hencky strains up to $\varepsilon_f \approx 6.3$ and elongational stretch rates of $0.1 \text{ s}^{-1} \leq \dot{\varepsilon}_0 \leq 20 \text{ s}^{-1}$. These limits were estimated based on an initial plate separation of $L_0 = 0.35 \text{ cm}$, and an endplate diameter of $D_0 = 0.35 \text{ cm}$, which are the values used for all of the experiments presented here.

As a fluid filament is stretched in the rheometer, the mid-filament diameter, D_{mid} , is measured in real time by a CCD laser micrometer (Keyence Model VG-301). Five thousand CCD elements in a 1-D linear array allow the diameter to be measured with a resolution of $\pm 10 \text{ }\mu\text{m}$. The total force, F_p , on the bottom endplate, is measured with a load cell (Futek Model L2338), which has a capacity of 10 grams and a resolution of $\pm 5 \text{ mg}$. The load cell design is based on strain-gage technology, and has a dynamic response that can be modeled by a 2-pole Butterworth filter. The static and dynamic response of this load cell has been fully characterized and will be reported in a separate note, including a discussion of the ramifications of performing transient force measurements with a mechanical measurement system [25].

All data relevant to the transient extensional rheology of the stretching filament, including total force on the endplate, mid-filament diameter, plate positions, and position errors, are gathered synchronously and in real-time by the PMAC motion controller. Video images of the deforming filament are simultaneously recorded in the stationary reference frame of the bottom endplate. During post-processing, raw force data is deconvolved from the response function of the load cell, as described in [25], and the processed data is then filtered using a moving average window of between 3 and 11 data elements. The raw mid-filament diameter data is fitted to a function comprised of a decaying exponential superposed with a low-order polynomial function. The effective

deformation rate, $\dot{\epsilon}_{eff}(t)$, is computed from this fitted function using equation (7). Finally, the transient Trouton ratio is computed as a function of Hencky strain via equations (10) and (11).

3.2. Rheology of Elastic Test Fluids

The two fluids measured in the current study are constant-viscosity, ideal-elastic Boger fluids. The polystyrene-based fluid consists of a high molecular weight polystyrene with a narrow polydispersity index (Scientific Polymer Products, $M_w = 2.25 \times 10^6$ g/mol, $PDI = 1.02$) dissolved in oligomeric styrene (Hercules Piccolastic A5) at a concentration of 0.05 wt.%. The extensional rheology of this fluid was previously considered by Spiegelberg and McKinley, and is denoted PS-05 [8]. The polyisobutylene-based fluid was also previously considered by Spiegelberg *et al.*, and is denoted BG-1 [7]. The fluid consists of 0.31 wt.% high molecular weight PIB (Exxon Vistanex L-120, $M_w \approx 1.8 \times 10^6$ g/mol) dissolved in 4.83 wt.% tetradecane (C14) and 94.86 wt.% polybutene (Amoco H100, $M_w \approx 900$ g/mol). While the high molecular weight polystyrene used in the PS-05 fluid is almost monodisperse, the polyisobutylene used in BG-1 is significantly more polydisperse.

Details of the fluid preparation and characterization for each of the above fluids can be found in [7] and [8]. The viscometric properties of the two fluids are summarized in Table 1, and the viscometric functions for PS-05 are shown in Figure 4. The Deborah number, or the ratio between the characteristic response time of the fluid and a characteristic time in the flow, is defined throughout this paper in terms of the commanded (or *constant*) deformation rate,

$$De = \lambda_s \dot{\epsilon}_0 \quad (12)$$

where $\dot{\epsilon}_0 = \dot{E}$ for a Type I/II experiment, and $\dot{\epsilon}_0 = \dot{\epsilon}_{eff}$ for a Type III experiment. The

relaxation time of the fluid that is used in this paper is computed from the zero-shear-rate viscometric properties,

$$\lambda_s = \frac{\Psi_{10}}{2(\eta_0 - \eta_s)}. \quad (13)$$

The temperature dependence of both fluids used in this study is described by an Arrhenius relationship, in which the viscosity at a given temperature T is related to the viscosity at a reference temperature T_0 by the ratio

$$a_T \equiv \frac{\eta_0(T)}{\eta_0(T_0)} = \exp\left[\frac{\Delta H}{R}\left(\frac{1}{T} - \frac{1}{T_0}\right)\right]. \quad (14)$$

The quantity $\Delta H/R$, known as the ‘‘activation energy for flow’’, is given in Table 1 for each fluid. This Arrhenius relationship allows measured material properties of a given fluid to be shifted to a master curve that corresponds to the reference temperature T_0 . All data reported in this paper, including both shear viscometric functions and transient extensional viscosities, have been shifted to correspond to data taken at the reference temperature $T_0 = 25$ °C according to these principles of time-temperature superposition [26].

4. Active Control Schemes for Filament Stretching Rheometers

As discussed in §2.2 of this paper, one ultimately wishes to perform an experiment that approximates the uniaxial elongational stretching of an axially-uniform cylinder as closely as possible. To achieve this, numerical simulations have shown that the mid-filament diameter must decrease according to equation (4) [16]. The first method examined in this study for prescribing such a flow involves controlling the mid-filament diameter via a real-time active control scheme.

The basic idea behind this control scheme is illustrated in a block diagram as shown in Figure 5. The actual mid-filament diameter is sampled at discrete, equally-spaced time

intervals, Δt , which can be adjusted to stabilize the control loop. At each time step, the measured diameter is compared to the ideal diameter for the corresponding elapsed time. The resulting error information is then used to compute the next commanded movement of the endplates.

Computing the desired motion of the endplates consists of two stages. In the first stage, the diameter error is used to compute the desired diameter at the next time step via a standard PID-type controller [29,30]. In general, the *desired* diameter at time $t_{i+1} = (i+1)\Delta t$ can be computed via

$$D_{cmd}(i+1) = D_{meas}(i) + K_p \delta D(i) + (K_D/\Delta t)[\delta D(i) - \delta D(i-1)] + (K_I \Delta t) \sum_{j=0}^i \delta D(j), \quad (15)$$

where $\delta D(i)$ is the error in the diameter, and K_p , K_D and K_I are the proportional, derivative, and integral controller gains, respectively. These gains are “tunable,” allowing the experimenter to find an optimal set of values that minimize the diameter error over the duration of the experiment and that yield a stable control system.

Each controller gain has a different physical effect on the control outcome. The *proportional* gain, K_p , adds a value proportional to the diameter error to the commanded diameter increment. Proportional gain acts analogously to a mechanical spring and determines the “stiffness” of the loop. Too low a value of K_p will result in a control loop which cannot react quickly enough to errors, but too high a value can lead to sustained oscillations in the measured diameter. The *derivative* gain, K_D , adds a value proportional to the derivative of the diameter error to the commanded diameter increment. The effect of derivative gain is analogous to a mechanical damper, lending stability to a proportional-only controller. Using a non-zero value of K_D will allow stability at higher values of K_p , but using too high a value of K_D can again lead to instability, since small errors in the measurement system will be amplified by the differentiation process.

Finally, the *integral* gain, K_I , adds a term proportional to the cumulative integral over the diameter error to the commanded diameter increment. The effect of integral gain is to eliminate steady state, or slowly-varying, errors in the diameter, and allows the diameter to change even if the instantaneous error is exactly zero. The proportional-integral-derivative (PID) controller is a standard, widely-used type of control. Further information about tuning such a controller or about the effects of each type of gain can be found in standard controls textbooks [29].

The second stage in computing the desired motion of the endplates involves converting the desired diameter $D_{cmd}(i+1)$ into a desired axial position increment ΔL_p at time $(i+1)\Delta t$, since the position of each motor is the quantity directly controlled in the filament stretching rheometer. This conversion is not simple, as it depends intimately on the response of the fluid filament to a given separation of the endplates. Discussions of the one-dimensional slender filament approximation in §2.1 have illustrated that this response can be quite complicated, and is certainly nonlinear. The simplest conversion method involves assuming the filament is deforming as a uniform cylinder, and thus, by manipulating equations (4), the plate separation will be related to the diameter according to

$$L_p(i+1) = L_p(i) \left[D_{meas}(i) / D_{cmd}(i+1) \right]^2. \quad (16)$$

Since the response of a fluid in a filament stretching rheometer is clearly *not* ideal, one needs a more accurate method of converting between the desired diameter and the endplate separation. At short times an obvious improvement would be to assume that the fluid follows the lubrication solution given in equations (5) for the reverse squeeze flow of a Newtonian fluid. In this case, the relationship becomes

$$L_p(i+1) = L_p(i) \left[D_{meas}(i) / D_{cmd}(i+1) \right]^{4/3}, \quad (17)$$

which has the same form as for the case of a uniform cylinder, but with a different value

of the exponent. Here and in what follows we assume that the desired (measured or commanded) value of D is at the axial midplane ($z = L_p(t)/2$) of the filament.

Although the response of a viscoelastic fluid should be considerably more complicated than either of the two cases already discussed, within the one-dimensional formulation given in equation (1), the desired relationship will have the same *form* as equations (16) and (17). Renardy [27] provides several numerical examples of how the Lagrangian stretch in a filament evolves as a function of time within this one-dimensional framework with no imposed stretching. Bousfield *et al.* [28] have also used a similar (Eulerian) 1-D formulation and show how well it can describe the non-linear evolution of Newtonian and viscoelastic liquid jets in both finite-element simulations and experimental observations. The form of equations (16) and (17) can be expected to hold at least locally in time, although the exponent will no longer be constant, but will instead vary with time, according to

$$L_p(i+1) = L_p(i) [D_{meas}(i)/D_{meas}(i+1)]^{p(i)} \quad (18)$$

Numerical simulations with different constitutive models can provide predictions for the evolution of $p(i)$. In the present work, the goal is to determine the evolution of the exponent $p(i)$ for an unknown material.

5. Open-Loop Control Using the Simple 1-D Formulation

The real-time active control scheme outlined in the previous section, although effective in achieving a temporally homogeneous mid-filament diameter profile, exhibits behavior characteristic of all such control systems: *it oscillates*. A PID controller determines its next step by examining an error signal, which leads to a measured signal that varies about a reference signal. Although this deviation may be very small, any fluctuation in the diameter profile will be amplified in the plate motion, as shown in

equations (16)-(18). Differentiation of rapid, small-amplitude position fluctuations leads to larger velocity fluctuations and even larger velocity gradient fluctuations. These fluctuations rapidly propagate through the viscous incompressible filament, causing large fluctuations in the total force exerted on the bottom endplate. Since the ultimate goal of the filament stretching experiment is to measure the transient force response, and thus the transient extensional viscosity of a fluid filament, the oscillations that naturally arise in a PID-type controller will undermine the desired goal, and are thus unacceptable. While the trial-and-error technique so often used in the past will certainly work, this method is tedious and time-consuming. One would like to find a new technique that will result in smooth force profiles while also reducing the time and effort involved in performing a single experiment. Fortunately, closer examination of the one-dimensional slender filament approximation embodied in equations (1) and (18) reveals a surprisingly simple procedure.

In the active control scheme of §4, we proposed a general relationship between the endplate separation and the midpoint diameter via equation (18). We can obtain more information about a specific form for this relationship by considering the general form of the velocity profile in the slender filament, given in equations (1). These may be rewritten in dimensionless form as

$$\begin{aligned} \mathbf{v}_z &= \dot{L}_p S(\zeta(t), t) \\ \mathbf{v}_r &= -\frac{1}{2} r \left(\frac{\dot{L}_p}{L_p} \right) S'(\zeta(t), t) \end{aligned} \quad (19)$$

where $\zeta(t) \equiv z/L_p(t)$ is a dimensionless axial position, $S(\zeta(t), t)$ is the instantaneous dimensionless axial velocity profile, and $S'(\zeta(t), t) \equiv (\partial S / \partial \zeta)_t$. Using the definition of the radial velocity at the axial midpoint of the free surface ($z = 0$, $r = D_{mid}/2$), we find that the mid-filament diameter can be related to the plate separation by the following equation:

$$\frac{dD_{mid}}{dt} = -\frac{1}{2} D_{mid} \left(\frac{\dot{L}_p}{L_p} \right) S'(0,t), \quad (20)$$

where the midplane of the filament is always located at $\zeta = 0$.

Using definitions of the imposed axial elongation rate $\dot{E}(t) = \dot{L}_p/L_p$ and the effective deformation rate given in equation (7), we obtain a general relationship between the principal deformation rates in the experiment,

$$\frac{\dot{\epsilon}_{eff}(t)}{\dot{E}(t)} = S'(0,t). \quad (21)$$

Equations (20) and (21) show that the resulting midpoint diameter profile is related to the endplate separation profile through the dimensionless function $S'(0,t)$. In general, $S'(0,t)$ will depend on the constitutive response of the fluid, and on the specific applied deformation history. However, we expect that experiments on a given fluid with the same *nominal* strain rate should yield the same function $S'(0,t)$. We can thus use the above formulation to directly obtain the correct position profile for a Type III experiment, in which $\dot{\epsilon}_{eff}(t) = \dot{\epsilon}_0$, by simply *measuring and computing* $S'(0,t)$ from a Type II experiment, in which $\dot{E}(t) = \dot{\epsilon}_0$, which is straight-forward to impose.

At this point it is insightful to note that an empirical relationship between the endplate separation and the midpoint diameter has recently been noticed by other research groups [31,32]. Orr and Sridhar reported a method [32] in which they plot data for a given experiment as $\ln(L_p/L_0)$ vs. $\ln(D_0/D_{mid})$. Orr and Sridhar note that this curve, which compares two different measures of the Hencky strain in the filament, is observed to follow a ‘master curve’ for certain Boger fluids over a wide range of Deborah numbers. Orr and Sridhar use the ‘master curve’ generated in a Type II experiment to obtain the desired position profile for a Type III experiment by picking points along the curve that correspond to an exponentially-decreasing midpoint diameter.

The one-dimensional formalism introduced in the present paper incorporates the empirical method of Orr and Sridhar. The relationship between the two methods can be shown by reconsidering equation (20). Nondimensionalizing both sides by using L_0 and D_0 , and bringing both derivatives to one side, we obtain

$$\frac{\frac{d \ln(D_{mid}/D_0)}{dt}}{\frac{d \ln(L_p/L_0)}{dt}} = -\frac{1}{2} S'(0, t). \quad (22)$$

Eliminating dt and inverting leads to

$$\frac{d \ln(L_p/L_0)}{d \ln(D_0/D_{min})} = \frac{2}{S'(0, t)}. \quad (23)$$

Thus, we can see that the function $S'(0, t)$ can be determined by *differentiating* the ‘master curve’ of Orr and Sridhar. Finally, we note that although S' is apparently a function of *time* in equations (19), the form of equation (23) shows that we have effectively created a *parametric curve*, where *time* is an implicit parameter along a curve of $\ln(L_p/L_0)$ vs. $\ln(D_0/D_{mid})$. The function S' is more accurately written as a function of the current strain,

$$S'(0, t) = S'(0, t(D_{mid})) = S'(\ln(D_0/D_{mid})). \quad (24)$$

To illustrate the validity of this approach, we examine a prototypical response from an Oldroyd-B fluid. We simulate a Type II experiment by constructing a diameter profile of a qualitatively similar form to profiles observed experimentally. This diameter profile consists of a superposition of two decaying exponential functions,

$$D(t)/D_0 = (1 - a)e^{-b\dot{E}t/2} + ae^{-\dot{E}t/2b} \quad (25)$$

where $a \approx 0.3$ and $b \approx 1.5$. This functional form is related to the endplate position formula typically used in a trial-and-error approach [7]. The instantaneous effective

strain rate can now be computed by combining equations (7) and (25), and this effective strain rate can then be used when integrating the evolution equations for the stress in a spatially homogeneous cylindrical fluid element of an Oldroyd-B fluid which is deforming with a temporally inhomogeneous strain rate [26].

We now compare the tensile stress profiles for the simulated Type II experiment discussed above and a simulated Type III experiment in which the strain rate is constant. Figure 6 (a) and (b) shows the diameter profiles and the tensile stress profiles, respectively, which correspond to simulated Type II and III experiments for $De = 4.64$. The two stress profiles will be qualitatively distinct if they are plotted as functions of *time*. However, at all moderate and large Deborah numbers ($De > 0.5$), the curves will superimpose if plotted as functions of *Hencky strain* ϵ_D (based on the actual diameter profile, cf. Eq. (11)), as illustrated in the figure. This universal response for stress is analogous to the master curve of Orr and Sridhar which was based on the flow kinematics, and also helps motivate the need to express the function S' as a function of the current strain, ϵ_D . Our earlier assumption that the function $S'(\epsilon_D)$ should be the same for two different types of experiments at the same *nominal* stretch rate will hold for fluids whose rheological response is governed primarily by the current strain, as is the case for an Oldroyd-B fluid when $De \geq 0.5$. Thus, we expect the one-dimensional formulation we have discussed here will work for Boger fluids, since measured transient extensional viscosities for these fluids have been observed to nearly superimpose when plotted as functions of Hencky strain [7,8]. However, the technique would not be expected to work for fluids whose response is governed by other forces, such as a Newtonian filament with aspect ratio $\Lambda \gg 1$, or for materials whose structure changes with time, such as a thermosetting resin.

In this section, we have shown that a one-dimensional approximation of the stretching filament can be used to obtain a general relationship between the endplate separation and the midpoint diameter in a filament stretching experiment. This general relationship suggests a very simple method for computing the complicated endplate position profile needed to obtain an exponentially-decreasing midpoint diameter. Although the function relating $L_p(t)$ and $D_{mid}(t)$ is unknown in general, it is easily *measured* by imposing a known function for the endplate separation, $L_p(t) = L_0 \exp(\dot{E}t)$ and recording $D_{mid}(t)$. The computation to obtain the desired position profile can be approached in two different ways. The first approach computes a Type III position profile using the two characteristic *strain rates* of the stretching experiment, $\dot{E}(t) = \dot{L}_p/L_p$ and $\dot{\epsilon}_{eff}(t)$ (equation (7)). The second approach, on the other hand, uses the two characteristic *Hencky strains* in the stretching filament, $\epsilon_L = \ln(L_p/L_0)$ and $\epsilon_D = 2 \ln(D_0/D_{mid})$. In both methods, equations (21) and (23), respectively, can be combined with equation (24) and then integrated to obtain the desired position profile,

$$L_p^{(III)} = L_0 \exp \left\{ \int \left(S'(\epsilon_D^{ideal}) \right)^{-1} d\epsilon_D^{ideal} \right\}. \quad (26)$$

where $\epsilon_D^{ideal} = \dot{\epsilon}_0 t$, and $d\epsilon_D^{ideal} = \dot{\epsilon}_0 dt$. The computed endplate separation can then be downloaded to the motion controller for the filament stretching device. In the following section, we present some results using these methods for two different Boger fluids, and we evaluate the accuracy of this method as compared to other heuristic methods used in the past.

6. Results and Discussion

In this section, we present results for Type III filament stretching experiments, obtained by both the real-time active control method described in §4, and the open-loop method described in §5. Comparisons of mid-filament diameter profiles and endplate position profiles for the two methods illustrate the oscillations that naturally occur in an

active control loop. We compare total force profiles for Type II and III experiments using the open-loop method, and finally, we compare transient Trouton ratios for Type II and III experiments for two different Boger fluids.

6.1 *Closed Loop Control*

Tuning of the real-time active control loop is illustrated in Figure 7(a). The fluid used is a polystyrene-based Boger fluid with a similar formulation to the PS-05 fluid, but with a lower concentration (0.025 wt.%) of high-molecular weight polystyrene. Tuning results were found to be relatively independent of the imposed stretch rate and of the fluid formulation. The update time of the control loop was set to 50 ms; smaller time increments were found to be dynamically unstable. Two Type II experiments are shown in the figure for comparison purposes, the first with an imposed stretch rate \dot{E} equal to the desired deformation rate $\dot{\epsilon}_0$, and the second with an imposed stretch rate equal to *two-thirds* of the desired deformation rate (cf. Eq. (7)). Results from these two experiments show that since the fluid velocity field is initially described by the Newtonian lubrication response given in equation (5), a good first step toward achieving the desired deformation rate is to simply impose a slower stretch rate. However, once strain hardening begins to occur for the Boger fluid at a Hencky strain $\epsilon \approx 2$, neither Type II experiment can maintain a constant effective deformation rate, $\dot{\epsilon}_{eff}$. Active control results using the three formulas for converting desired mid-filament diameter into desired endplate position, given in equations (16), (17), and (18), are also shown in the figure. All three mechanisms produce diameter profiles that are closer to the targeted exponential decrease than a simple Type II experiment yields. However, as with the Type II experiments, once strain hardening begins, the first two formulations are unable to maintain the desired diameter profile. The general formulation given in equation (18) allows the control system to maintain a nearly ideal diameter profile over the duration of the experiment.

The success of the active control method becomes clearer through examination of diameter error profiles, as illustrated in Figure 7(b). The actual diameter measured in a Type II experiment can drift away from the ideal curve by as much as 40%, although the diameter again approaches the target profile at higher Hencky strains. Figure 7(b) shows that all three methods of converting between desired diameter and desired position yield relatively small diameter errors up to a Hencky strain of approximately 2. Beyond this point, the polymeric stresses arising from the onset of strain hardening in the fluid overwhelm the stresses in the Newtonian solvent, and the first two overly-simplistic control schemes cannot cope with such rapid changes in the fluid response. These two control schemes are able to control the diameter to within an absolute deviation from the ideal curve of 8% over most of the duration of the experiment, but this deviation increases to 20% at later times. The third method, which implements a time-varying relationship between mid-filament diameter and endplate position, is able to improve the late-time deviation to less than 15%.

6.2 *Open-Loop Control*

As discussed in §5, the fluctuations inherent in the active control loop cause significant oscillations in the measured tensile force. In order to circumvent these undesirable fluctuations, we now examine the open-loop technique described in §5. The first step in the process is to perform a Type II experiment, and then compute the function $S'(\epsilon_D)$ via equations (21) and (24). Figure 8 shows the resulting function $S'(\epsilon_D)$ for various applied stretch rates for the PS-05 Boger fluid and the BG-1 Boger fluid. At small strains, when the viscous response of the Boger fluid dominates, this ratio of deformation rates approaches $S' \cong 1.5$, which is the expected response of a Newtonian fluid in a reverse squeeze flow, given in equation (17). As the polymeric stresses grow, the actual radial contraction of the filament slows, S' begins to decrease, dropping below unity, and then increasing again and approaching unity at higher strains. Similar

behavior of the effective strain rate has previously been observed both experimentally [14] and numerically [18]. The plots in Figure 8 show that the response of both Boger fluids are weakly dependent on the imposed strain rate. While the form of $S'(\epsilon_D)$ remains qualitatively similar for each rate, the magnitude of the function for a fixed strain value decreases with increasing strain rate for each fluid. In addition, the onset of the sudden decrease in filament contraction rate shifts toward lower strains as the imposed strain rate increases. The trend is much more pronounced for the BG-1 fluid, indicating that the precise fluid response is also dependent on fluid formulation.

A second alternative method of representing the kinematic response of a fluid is shown in Figure 9. As discussed in §5, these figures compare two different characteristic Hencky strain measures for the elongating filament, one based on the endplate position, $\epsilon_L = \ln(L_p/L_0)$, and the second based on the decreasing midpoint diameter, $\epsilon_D = 2\ln(D_0/D_{mid})$. A similar ‘master curve’ for a fluid was first presented by Orr and Sridhar [32]. Figure 9(a) shows the ‘master curve’ for the PS-05 Boger fluid, and (b) shows the same function corresponding to the BG-1 Boger fluid. As we saw in Figure 8, the precise shape of the curve in fact depends on both the applied strain rate and on the fluid formulation.

Once the function $S'(\epsilon_D)$ has been computed, the next step toward performing a Type III experiment is to compute the desired endplate position profile using equation (26). A smooth endplate position profile for a Type III experiment computed using this procedure is shown in Figure 10 for the PS-05 Boger fluid for an applied strain rate of 3.0 s^{-1} . The curve of $S'(\epsilon_D)$ shown in Figure 8(a) for $\dot{\epsilon}_0 = 3.0 \text{ s}^{-1}$ is the same data used to generate this position profile. The endplate position profile resulting from the active control loop is shown for comparison. Although the closed-loop active control and open-loop profiles follow similar trends, the oscillations in the active control case are noticeable and the

endplate position deviates dramatically from the smooth profile well before the end of the experiment, indicating that the active control loop became unstable. In addition to being unstable, the position oscillations also lead to accelerations and velocities that rapidly exceed the motion control system limits. Thus, the active control scheme is limited not only by the undesirable force oscillations that are transmitted through the viscous filament from the oscillating endplates, but it is also limited to only moderate strains due to its unstable nature and due to mechanical system limitations. In contrast, the open-loop technique leads to smooth profiles that can be reliably and repeatedly performed by the motion control system.

Figure 11(a) and (b) illustrates the success of the open loop technique in prescribing an ideal mid-filament diameter profile. The diameter profiles shown are those resulting from the application of the endplate position profiles shown in Figure 10. The actual diameter profile for this Type III experiment is visually indistinguishable from the desired profile, and the error profile is much smoother than that resulting from active control. Although the technique is open loop, with no means for correcting the deformation of the filament in real time, the resulting diameter error remains under 2% for most of the duration of the experiment, while the diameter itself has decreased by an order of magnitude and the filament length has increased by two orders of magnitude. The slight increase in the diameter error (still under 10%) at later times is due mainly to instrument noise in the CCD laser micrometer, which becomes proportionally larger in the final 0.3 seconds of this experiment as the diameter approaches the minimum specification of the device (500 μm). These errors can be readily reduced by using a more sensitive measuring device.

6.3 Extensional Stress Growth

Now that we have confirmed that Type III experiments can be successfully performed using our one-dimensional open loop technique, we examine the rheological response of the test fluids to both Type II and Type III experiments. The final experimental quantity that we measure during the filament stretching experiment is the axial force exerted on the bottom endplate. Figure 12 compares the transient force profiles for an applied strain rate of $\dot{\epsilon}_0 = 3.0 \text{ s}^{-1}$ for Type II and III experiments for both Boger fluids. The force data has been deconvolved from the transducer response function and filtered as described in §3.1. The typical qualitative response of a Boger fluid is seen in these profiles, in which there is an initial overshoot and subsequent decrease in the tensile force at early times due to the dominant response of the Newtonian solvent. At intermediate times, strain hardening becomes apparent and the force begins to rise again. Finally, at later times, the force reaches a maximum and gradually begins to decrease as the stress in the fluid reaches steady state.

Although the qualitative dynamical response is similar for both fluids and for both types of experiments, the curves in Figure 12 are quantitatively distinct. The local minima in the force curve for Type III experiments (hollow symbols) are shifted toward later times, and the magnitude of the second maximum increases slightly. Finally, the magnitude of the tensile force in the lower molecular weight, polydisperse BG-1 fluid is nearly an order of magnitude smaller than that measured in the PS-05 fluid.

Finally, we present the transient Trouton ratios for the two Boger fluids computed using equation (10). We first show results comparing Type II and III experiments for a rate of 3.0 s^{-1} for both fluids in Figure 13. Results measured using the open loop technique described above agree well with those measured previously by Spiegelberg *et al.* [7,8] for both fluids. However, to obtain such profiles previously required repeated

use of a ‘trial-and-error’ method based on the dual-exponential approach we discuss in §5. By contrast, the technique presented here requires only two steps. The new results presented here also extend the transient curve up to a Hencky strain of approximately $\varepsilon_D \cong 5.7 \pm 0.1$, allowing the evolution of stresses toward steady state to be observed. The Type III experiment leads to a different transient growth of the Trouton ratio compared to the Type II experiment, primarily modifying the shape of the curve at intermediate strains. The trends observed in the data presented here for Type II and III experiments are consistent with those indicated by the simulations of Kolte *et al.* [16]. The discrepancy between our Type III results and those previously reported by Spiegelberg *et al.* [7,8] at intermediate strains illustrates the sensitivity of the rheological response of a fluid filament to slight changes in the shape of the imposed position profile. This sensitivity drives the need to obtain accurate diameter and force measurements so that accurate Type III position and Trouton ratio profiles can be computed.

In Figure 14(a) and (b) we compare the results from the Type III experiments for several different applied strain rates for each fluid. The three curves for the PS-05 fluid, corresponding to Deborah numbers of $De = 2.50$, $De = 6.80$ and $De = 11.3$, respectively, nearly superimpose, a phenomenon that has also been observed by numerous other research groups [5-14]. The experimental curves do not exactly superimpose, however, exhibiting a more rapid stress growth as the Deborah number increases. This trend is consistent with expectations from simulations using simple dumbbell models, which also show a delayed linear viscoelastic response at short times as the Deborah number increases (when plotted as a function of strain rather than t/λ_s). The approach to steady state is much more gradual than was reported in early filament stretching experiments (e.g. Tiratmadja and Sridhar [6]), but this is also consistent with Brownian dynamics calculations and single chain experiments that reflect the non-Gaussian distribution of individual trajectories of the chains [33,34]. For the semi-dilute polydisperse PIB fluid, BG-1, there is even less superposition in the data curves, which

correspond to Deborah numbers of $De = 1.01, 2.44,$ and $4.03,$ respectively. The steady state Trouton ratio approached by the PS-05 fluid appears to be approximately the same for all three Deborah numbers, while the BG-1 fluid still has not begun to reach steady state even at a Hencky strain of $\epsilon_D \approx 5.8.$

Finally, Figure 15 directly compares the transient Trouton ratio profiles for the two different Boger fluids. Since the Deborah numbers corresponding to the same applied strain rates are significantly higher for the PS-05 fluid, it is not surprising that the slopes in the growth region are steeper for this fluid. The lack of a definite steady state plateau for the BG-1 fluid can be attributed to the polydispersity of the high molecular weight polyisobutylene in the solution [35]. In contrast, the high molecular weight polystyrene in the PS-05 solution is very monodisperse, allowing the finite extensibility of the chains to be sensitively probed.

7. Conclusions

We have presented two new techniques for obtaining the desired kinematics in a filament stretching device. The first technique is an active, ‘closed-loop’ control loop in which the mid-filament diameter is observed in real-time and the diameter error information is used to change the controlled position profile on-the-fly. This active control scheme allows the diameter to be controlled to within 15% error for the duration of the experiment. However, oscillations characteristic of this and many other active control systems proved to be unacceptable, both in obtaining smooth transient force measurements, and in realizing the potential operating range of the filament stretching rheometer.

The second technique, while essentially open loop, utilizes a one-dimensional analysis of the kinematic profile in the slender stretching filament to determine the

desired endplate separation as a function of time. A ‘Type II’ experiment, described in §2.2, is performed first, and measured values of the mid-filament diameter and endplate position profiles are used to compute *desired* endplate position profiles for a ‘Type III’ experiment. This procedure is significantly simpler to implement than either the active control technique described above, or the trial-and-error procedure employed by all practitioners of filament stretching rheometry in the past [5-14]. This systematic approach is logically connected to the empirical technique recently presented by Orr and Sridhar [32] and reviewed briefly in §5. Diameter profiles obtained using this method consistently agreed with the ideal diameter $D_{ideal}(t)$ to within $\pm 2\%$. This simple one-dimensional analysis demonstrates that, although the fluid behaves in a non-ideal way in a Type II experiment, this behavior is predictable and *unique*, containing all the information needed to prescribe a different set of kinematics in the stretching filament.

Although the techniques presented here for controlling the mid-filament diameter were tested on Boger fluids, both could work for other types of fluids, assuming that the solution for the filament deformation is unique and dominated by the total strain at $De > 0.5$ rather than by local variations in $\dot{\epsilon}_{eff}(t)$. In practice, the connection between the endplate displacement and the midplane strain experienced by the filament, which is represented by the function $S'(\epsilon_D)$, is governed by the constitutive response of the fluid. In particular, the one-dimensional slender filament theory of Renardy [22] shows that the evolution of the rate of change of the midplane ‘stretch’ or radius depends on the instantaneous tensile stress difference in the filament. For many viscoelastic materials in strong stretching flows with $De > 1$ the polymeric stress is primarily a function of strain (provided the strain rate is large and only varies slowly), and thus we expect our open-loop control strategy to be an effective way of determining the desired profile in a single iteration. The behavior of other types of fluids, such as Newtonian fluids and shear-

thinning fluids, are also of interest, and Type III experiments for these fluids will be presented in a later publication.

The active control technique presented here can also be extended to perform other types of controlled experiments, such as constant force and constant stress experiments. Such constant stress experiments, performed at low stretch rates in a similar filament stretching device that is appropriate for polymer melts, are presented by Münstedt *et al.* [37]. However, due to the short experimental duration of experiments with polymer solutions and the large instantaneous viscous stresses, oscillations will most likely still lead to undesirable fluctuations in the results for controlled stress experiments with more mobile fluids. Our active control scheme was based on very elementary principles of control theory, and a simple PID controller. This basic formulation assumes that the response functions of all the elements in the control system are linear, and that they can be compensated by the linear elements of a PID loop. However, we know that the actual fluid response is governed by the momentum equations and a constitutive relationship between stress and deformation. These coupled equations are nonlinear, and can in general display effects arising from coupling, hysteresis, and many other anomalous behaviors. Linear control methods are not optimal for such systems. More complicated methods involving nonlinear control theory will be more appropriate and could lead to better results than those presented here [40,41]. However, for the constant rate experiments given here, the one-dimensional open loop method is simple to implement, can be applied to a wide range of different control systems, and offers additional insights into the rheological behavior of the fluid. The errors in the actual diameter profile as compared to the target profile for this method are significantly smaller than those induced by the simple active control scheme.

Finally, we have also presented transient extensional rheology data for two different Boger fluids, using the open-loop technique described and a new filament stretching device with an extended operating range. The transient Trouton ratios for a polystyrene-based Boger fluid, previously investigated in [8], and for a polyisobutylene-based Boger fluid, previously investigated in [7], agree well with the previously reported data. The transient Trouton ratios for the monodisperse polymer solution nearly superimpose when plotted as a function of Hencky strain, which has been observed previously and is consistent with ideas of a large dissipative contribution to the stress [38,39].

Numerical simulations have indicated that performing a Type III experiment in a filament stretching rheometer will minimize the effect of the no-slip boundary conditions at the endplates and yield results that are virtually indistinguishable from those of an ideal, homogeneously deforming cylinder. This level of accuracy is desirable if detailed comparisons with theoretical constitutive models and simulations are to be made. The open-loop technique presented here provides a more accurate alternative to the tedious iterative method that has been used in the past to realize Type III experiments, and will hopefully be of use in the design and optimization of future filament stretching rheometers.

Acknowledgements

This research was supported by NASA under Grant No. NAG3-1385. S.L.A. thanks the Fannie and John Hertz Foundation for supporting her graduate research. S.L.A. would also like to thank Dr. Stephen Spiegelberg and Dr. Gavin Braithwaite for sharing their insight and experience with extensional rheology, controls, and experimental technique.

References

- [1] T.T. Perkins, D.E. Smith, and S. Chu in: H.K. Kausch, T.Q. Ngoyen (Eds.), *Flexible Chain Dynamics in Elongational Flows*, Springer-Verlag, Berlin, Heidelberg, 1998.
- [2] R.K. Gupta and T. Sridhar, in A.A. Collyer, D.W. Clegg (Eds.), *Rheological Measurement*, Elsevier Applied Science, London, 1988, pp. 211-245.
- [3] D.F. James and K.A. Walters, *Techniques in Rheological Measurement*, Elsevier, London, 1993.
- [4] J.E. Matta and R.P. Tytus, *J. Non-Newtonian Fluid Mech.* 35 (1990) 215.
- [5] T. Sridhar, V. Tirtaatmadja, D.A. Hguyen and R.K. Gupta, *J. Non-Newtonian Fluid Mech.* 40 (1991) 271.
- [6] V. Tirtaatmadja and T. Sridhar, *J. Rheol.* 37 (1993) 1081.
- [7] S.H. Spiegelberg, D.C. Ables and G.H. McKinley, *J. Non-Newtonian Fluid Mech.* 64 (1996) 229.
- [8] S.H. Spiegelberg and G.H. McKinley, *J. Non-Newtonian Fluid Mech.* 67 (1996) 49.
- [9] R. Kröger, S. Berg, A. Delgado, H.J. Rath, *J. Non-Newtonian Fluid Mech.* 45 (1992) 385.
- [10] S. Berg, R. Kröger, H.J. Rath, *J. Non-Newtonian Fluid Mech.* 55 (1994) 307.
- [11] M.J. Solomon and S.J. Muller, *J. Rheol.* 40 (1996) 837.
- [12] A. Jain, D.S. Shackelford and K.W. Koelling, *The 68th Society of Rheology Annual Meeting* (1997).
- [13] J. van Nieuwkoop and M.M.O. Muller von Czernicki, *J. Non-Newtonian Fluid Mech.* 67 (1996) 105.
- [14] M.R.J. Verhoef, B.H.A.A. van den Brule and M.A. Hulsen, submitted to *J. Non-Newtonian Fluid Mech.* (1997).
- [15] R.W. Shipman, M.M. Denn, and R. Keunings, *J. Non-Newtonian Fluid Mech.* 40 (1991) 281.
- [16] M.I. Kolte, H.K. Rasmussen and O. Hassager, *Rheol. Acta* 36 (1997) 285.

- [17] P. Szabo, *Rheol. Acta*, 36 (1997) 277.
- [18] M. Yao and G.H. McKinley, *J. Non-Newtonian Fluid Mech.* 74 (1998) 47.
- [19] D.O. Olagunju, submitted to *J. Non-Newtonian Fluid Mech.*
- [20] R. Sizaire and V. Legat, *J. Non-Newtonian Fluid Mech.* 71 (1997) 89.
- [21] S. Gaudet, G.H. McKinley and H.A. Stone, *Phys. Fluids* 8 (1996) 2568.
- [22] M. Renardy, *J. Non-Newtonian Fluid Mech.* 51 (1994) 97.
- [23] J. Eggers, *Rev. Mod. Phys.* 69 (1997) 865.
- [24] O. Harlen, *The 70th Society of Rheology Annual Meeting* (1998).
- [25] S.L. Anna, E. Anderson and G.H. McKinley, in preparation for *J. Non-Newtonian Fluid Mech.* (1998).
- [26] R.B. Bird, R.C. Armstrong and O. Hassager, *Dynamics of Polymeric Liquids. Volume 1: Fluid Mechanics*, Wiley-Interscience, New York, 1987.
- [27] M. Renardy, *J. Non-Newtonian Fluid Mech.*, 59 (1995) 267.
- [28] D.W. Bousfield, R. Keunings, G. Marrucci, and M.M. Denn, *J. Non-Newtonian Fluid Mech.*, 21 (1986) 79.
- [29] K. Ogata, *Modern Control Engineering*, 2nd Ed., Prentice Hall, Englewood Cliffs, New Jersey, 1990, Chapter 3.
- [30] PMAC Software Reference, Delta Tau Data Systems, Northridge, California, 1996, Chapters 3 and 5.
- [31] T. Sridhar, *personal communication*, (1998).
- [32] N.V. Orr and T. Sridhar, *J. Non-Newtonian Fluid Mech.*, *in press*, 1998.
- [33] R. Keunings, *J. Non-Newtonian Fluid Mech.*, 68 (1997) 85.
- [34] D.E. Smith and S. Chu, *Science*, 281 (1998) 1335.
- [35] J. Remmelgas, L.G. Leal, N.V. Orr, and T. Sridhar, *J. Non-Newtonian Fluid Mech.*, 76 (1998) 111.
- [36] M. Yao, G.H. McKinley, and B. Debbaut, *J. Non-Newtonian Fluid Mech.*, 79 (1998) 469.

- [37] H. Münstedt, S. Kurzbeck, L. Egersdörfer, *Rheol. Acta*, 37 (1998) 21.
- [38] J.M. Rallison, *J. Non-Newtonian Fluid Mech.*, 68 (1997) 61.
- [39] P.S. Doyle, E.S.G. Shaqfeh, G.H. McKinley, and S.H. Spiegelberg, *J. Non-Newtonian Fluid Mech.*, 76 (1998) 79.
- [40] D. Graham and D. McRuer, *Analysis of Nonlinear Control Systems*, John Wiley & Sons, Inc., New York, 1961.
- [41] J.M. Skowronski, *Control of Nonlinear Mechanical Systems*, Plenum Press, New York, 1991.

Captions

- Figure 1.** Sketch of a filament stretching apparatus. The origin is taken to be at the axial midplane of the filament.
- Figure 2.** Schematic diagram of the filament stretching rheometer: (a) linear DC brushless motor; (b) upper motor, with top endplate assembly; (c) lower motor, with diameter measurement assembly; (d) fluid sample; (e) force transducer, (f) CCD laser micrometer, transmitter, (g) receiver; (h) CCD camera.
- Figure 3.** Operating diagram for the filament stretching rheometer. This figure shows the range of velocities and endplate separations achievable in the current device, with corresponding Hencky strains shown along the top axis. The small box at lower left shows the operating space for a previous device [7].
- Figure 4.** Viscometric functions for a monodisperse 0.05 wt.% polystyrene-based Boger fluid, PS-05, measured in a cone-and-plate rheometer. Solid symbols represent the measured dynamic properties, while the hollow symbols represent measured steady shear properties. Solid lines show predictions for the viscometric functions using a FENE-P model, and dashed lines show the linear viscoelastic predictions of the Zimm model.
- Figure 5.** Block diagram showing an active control scheme for a *Type III* experiment in a filament stretching rheometer.
- Figure 6.** (a) Diameter profiles used to simulate Type II (\circ) and Type III (solid line) experiments, and (b) Tensile stress profiles for an Oldroyd-B model using the instantaneous effective strain rates computed from these diameter profiles.
- Figure 7.** (a) Diameter and (b) fractional error in the diameter illustrating the tuning process for an active control loop designed to yield a Type III experiment with $\dot{\epsilon}_0 = 2.0 \text{ s}^{-1}$. Dark solid line shows the ideal, target diameter profile; (+) symbols show data points from a Type II experiment with $\dot{E} = 2.0 \text{ s}^{-1}$; (\circ) symbols show results from a Type II experiment with $\dot{E} = 2/3(2.0) \text{ s}^{-1} = 1.33 \text{ s}^{-1}$; thin solid lines show results of active control experiments using various formulae for converting between desired diameter and desired endplate position. (*dash*: ideal cylinder, equation (16); (\circ): lubrication solution, equation (17); (\triangle): general form, equation (18)).

- Figure 8.** Computed strain rate ratio for Type II experiments, given by the function $S'(\epsilon_D)$ in equations (21) and (24). Results for three different applied stretch rates are shown for (a) the PS-05 and (b) the BG-1 Boger fluids: (○) 1.0 s^{-1} , (△) 3.0 s^{-1} , and (◇) 5.0 s^{-1} . Dashed lines mark ideal homogeneous uniaxial deformation, in which the radial contraction rate is equal to half of the axial stretch rate ($S'(\epsilon_D) = 1$), and the lubrication solution for a Newtonian fluid with exponentially stretching endplate boundary conditions imposed ($S'(\epsilon_D) = 1.5$).
- Figure 9.** ‘Master curve’ profiles showing the Hencky strain, ϵ_L (based on endplate position) as a function of the Hencky strain, ϵ_D (based on midpoint diameter) for (a) PS-05 and (b) BG-1 Boger fluids for the same applied stretch rates shown in Figure 7.
- Figure 10.** Endplate position profiles for Type II and III experiments with the PS-05 Boger fluid (nominal strain rate of 3.0 s^{-1}). The solid dark line corresponds to a Type II experiment; the (○) symbols show a Type III experiment performed via the active control scheme; and the dashed line shows the Type III position profile computed via the one-dimensional open-loop scheme. Smooth curves result from the open-loop scheme, while the active control loop leads to undesirable oscillations.
- Figure 11.** (a) Diameter profiles and (b) fractional diameter error profiles for a nominal strain rate of 3.0 s^{-1} , illustrating that a simple one-dimensional analysis yields a diameter profile that is within $\pm 2\%$ of the desired profile over most of the duration of the experiment, while the active control loop can only control the diameter to within 15% over the duration of the experiment. The solid dark line shows the target diameter profile; (△) symbols show the Type II experiment profile and (●) symbols show the Type III experiment profile resulting from the one-dimensional open loop scheme. The thin solid line shows the profile resulting from the active control scheme.
- Figure 12.** Force profiles comparing Type II experiments (filled symbols) and Type III experiments (hollow symbols) for an imposed strain rate of $\dot{\epsilon}_0 = 3.0 \text{ s}^{-1}$. (○) symbols show force profiles for the PS-05 Boger fluid, which are nearly an order of magnitude larger than those of the BG-1 Boger fluid, (△) symbols.
- Figure 13.** Transient Trouton ratio curves for (a) PS-05 Boger fluid and (b) BG-1 Boger fluid. The nominal applied strain rate is $\dot{\epsilon}_0 = 3.0 \text{ s}^{-1}$. Solid symbols (◆) show Type III results previously reported in [7,8] for the same fluids, performed via the traditional ‘trial-and-error’ approach. Hollow symbols show Type II results performed by the author (△), and Type III results performed via the one-dimensional open-loop scheme (○). The dashed line marks a Trouton ratio of $Tr = 3$.

Figure 14. Transient Trouton ratio curves for (a) the PS-05 Boger fluid and (b) the BG-1 Boger fluid for Type III experiments at different applied strain rates. Symbols correspond to stretch rates of $(\circ) 1.0 \text{ s}^{-1}$, $(\triangle) 3.0 \text{ s}^{-1}$, $(+) 5.0 \text{ s}^{-1}$. These correspond to Deborah numbers of $De = 2.50, 6.80,$ and 11.3 for the PS-05 fluid and $De = 1.01, 2.44,$ and 4.03 for the BG-1 fluid after using time-temperature superposition to correct for temperature deviations on the day of the test. The dashed line marks a Trouton ratio of $Tr = 3$.

Figure 15. Comparison of transient Trouton Ratios for PS-05 (\circ) and BG-1 (\bullet) Boger fluids for similar applied strain rates. (\circ) symbols correspond to $\dot{\epsilon}_0 = 1.0 \text{ s}^{-1}$, (\triangle) symbols to $\dot{\epsilon}_0 = 3.0 \text{ s}^{-1}$, and (\diamond) symbols to $\dot{\epsilon}_0 = 5.0 \text{ s}^{-1}$.

Table 1. Zero-shear-rate viscometric properties for a polystyrene-based Boger fluid, PS-05 (0.05 wt.%), a polyisobutylene-based Boger fluid, BG-1 (0.31 wt.%), and a viscous polystyrene oil at a reference temperature of $T_0=25$ °C.

Material Property	PS-05	BG-1	PS Oil
η_0 [Pa s]	38.0	13.8	
η_s [Pa s]	32.5	8.10	32.5
Ψ_{10} [Pa s ²]	20.0	8.96	
λ_s [s]	1.78	0.76	
$\Delta H/R$ [K]	19400	7360	19400

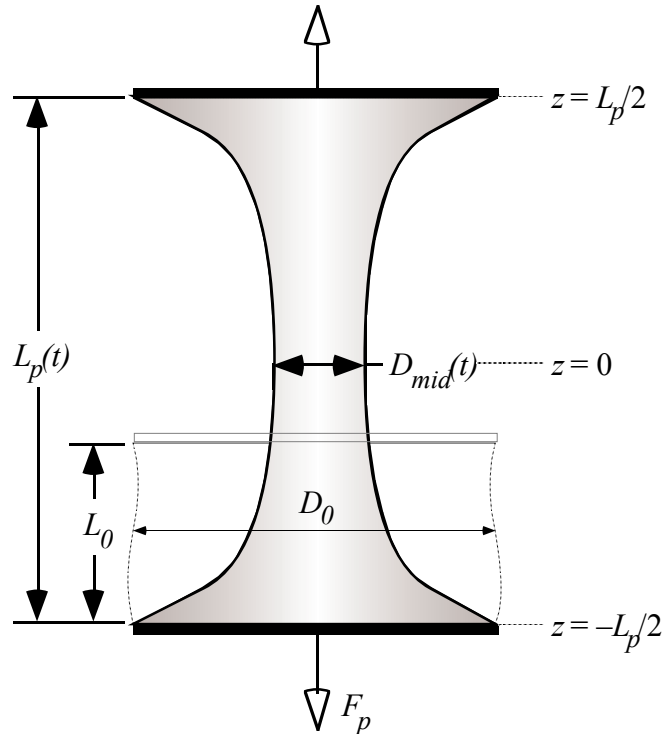


Figure 1

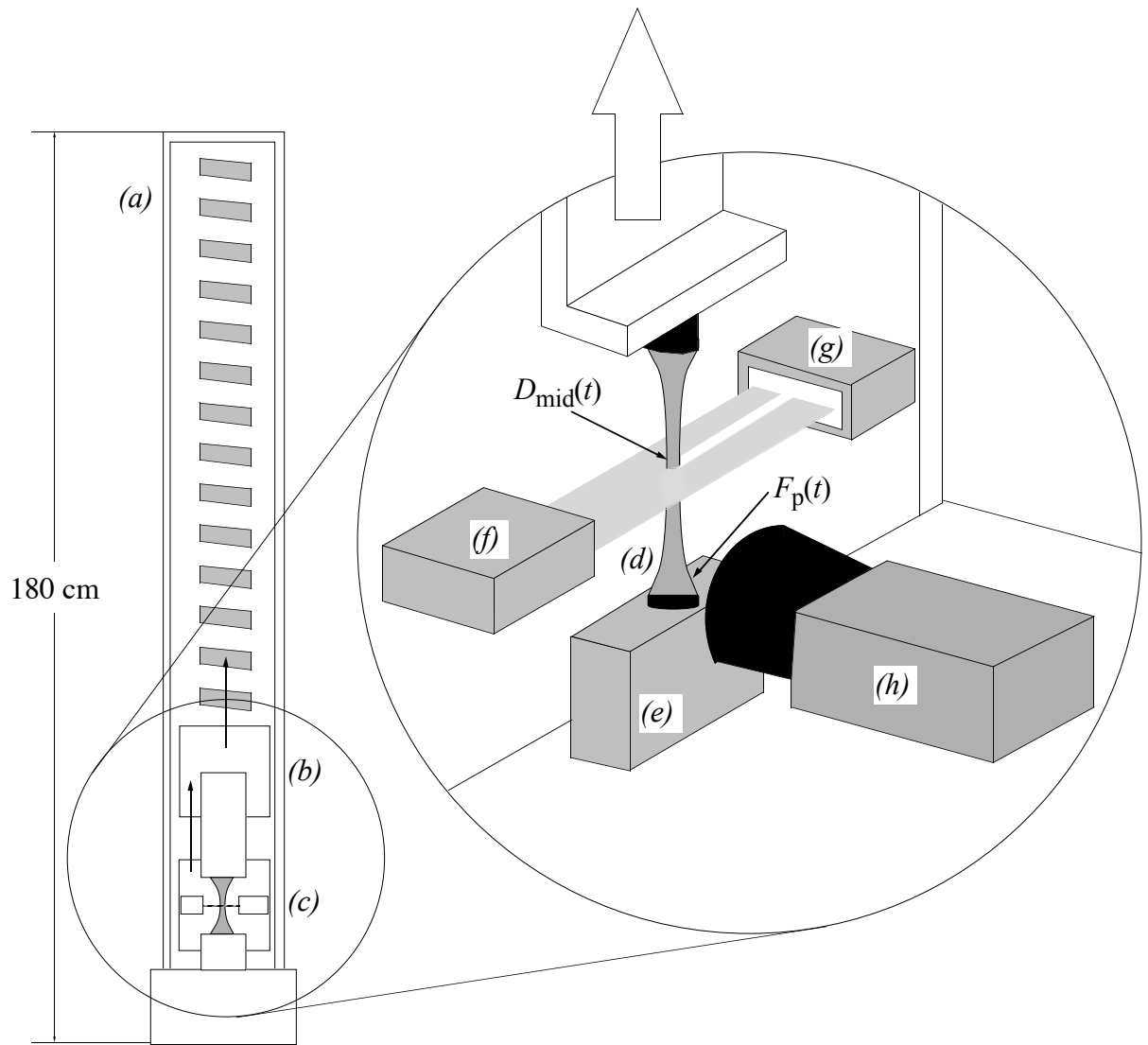


Figure 2

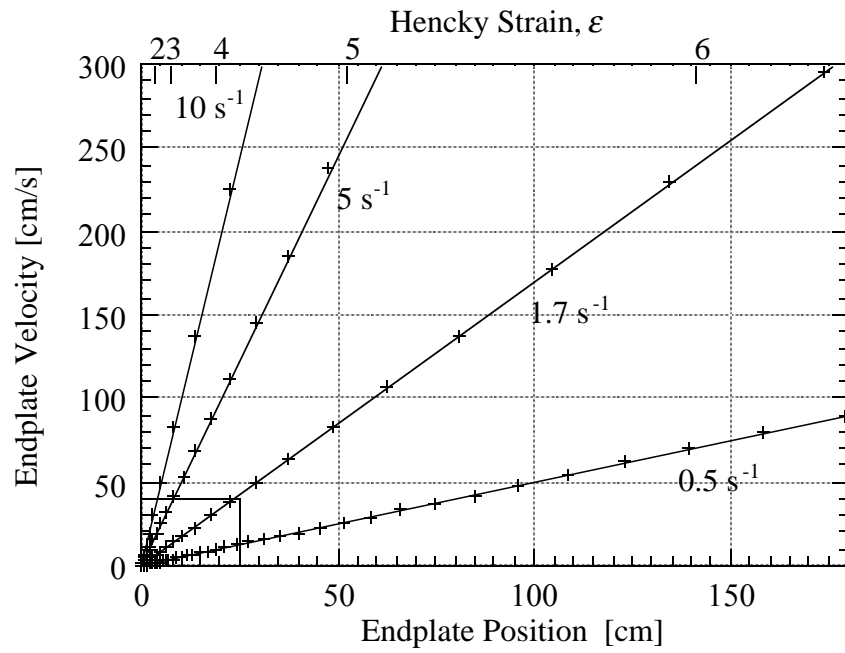


Figure 3

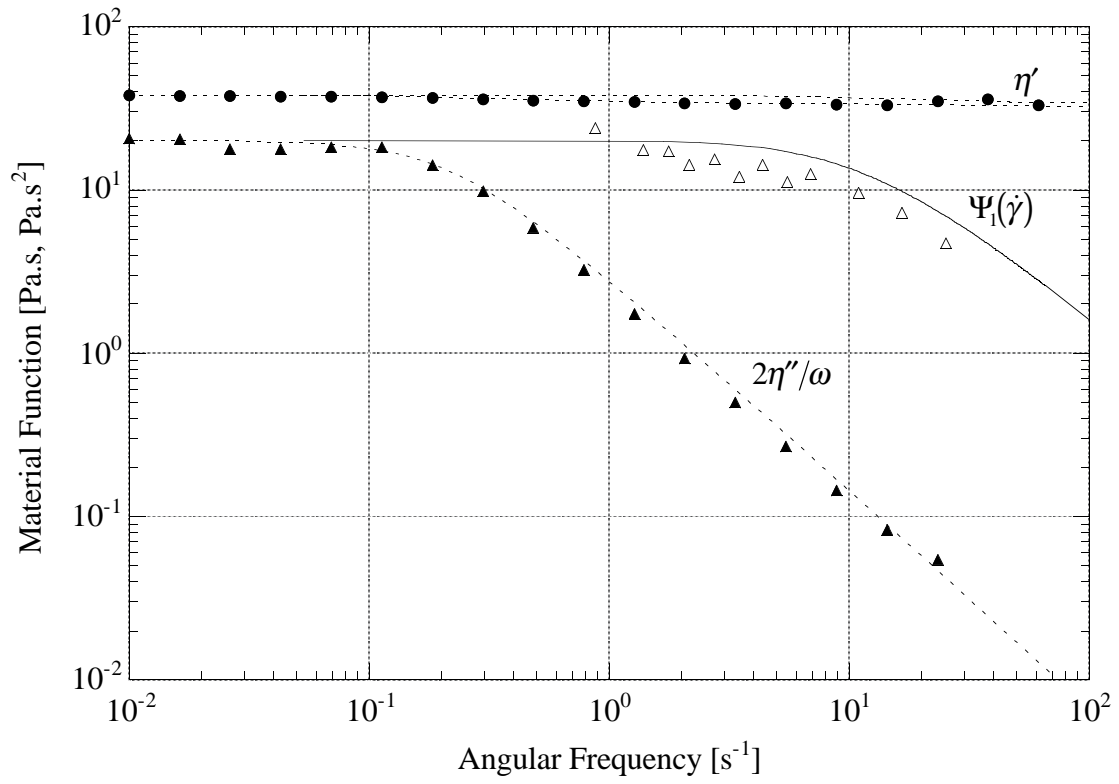


Figure 4

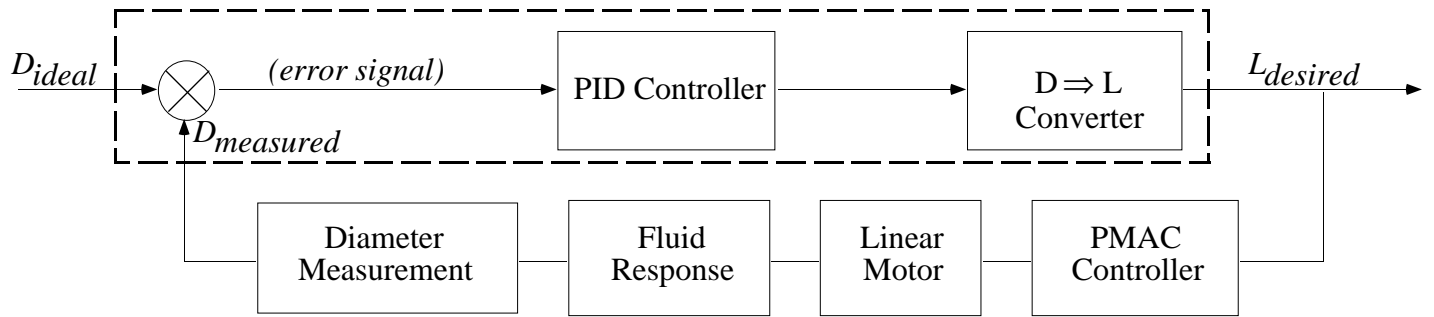


Figure 5

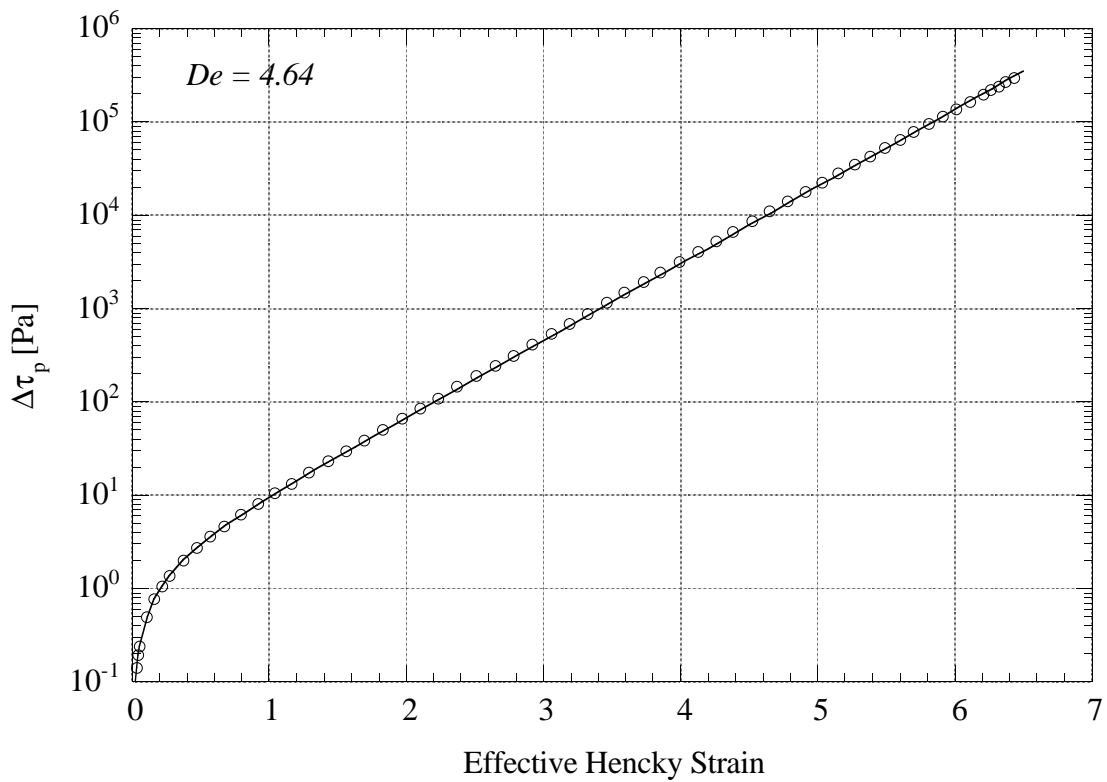
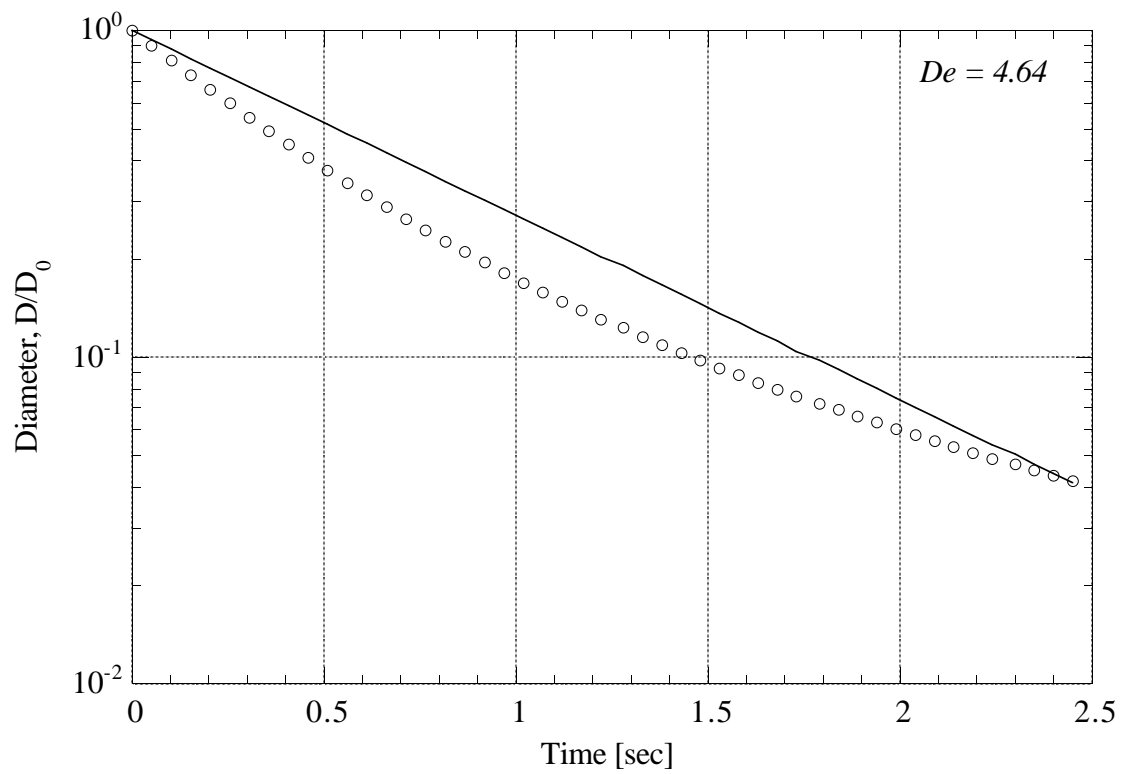


Figure 6

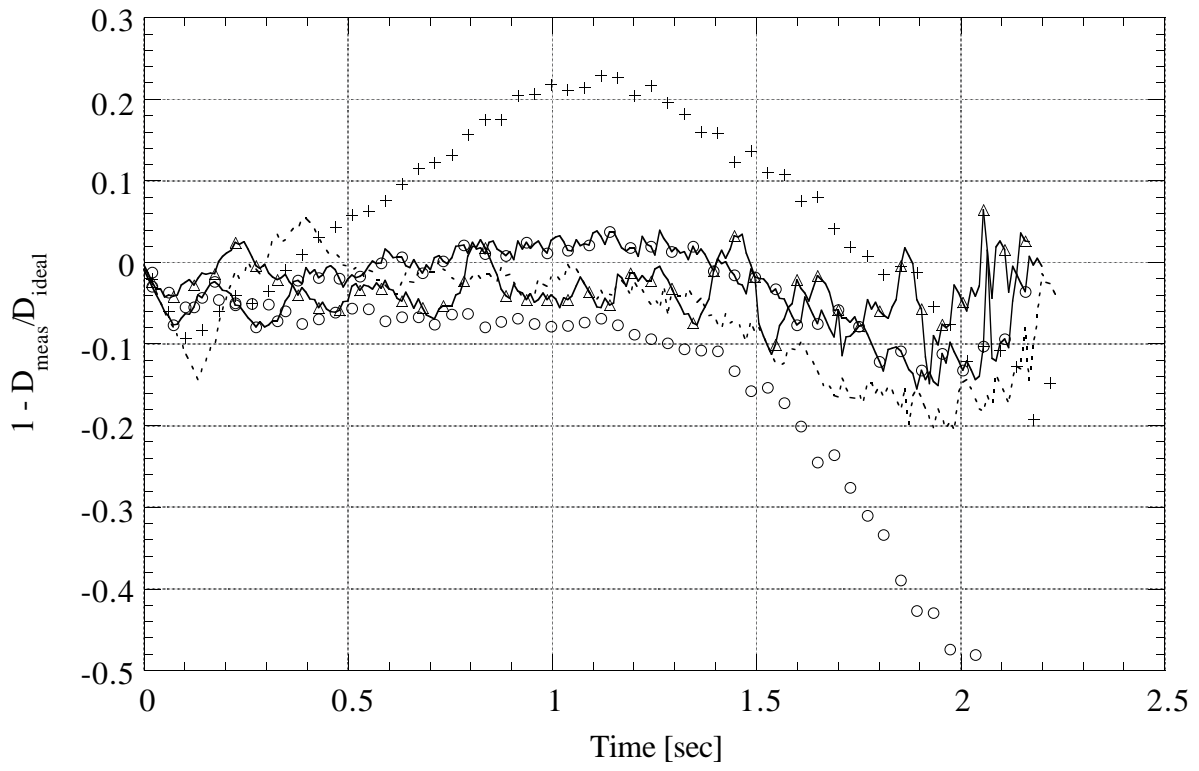
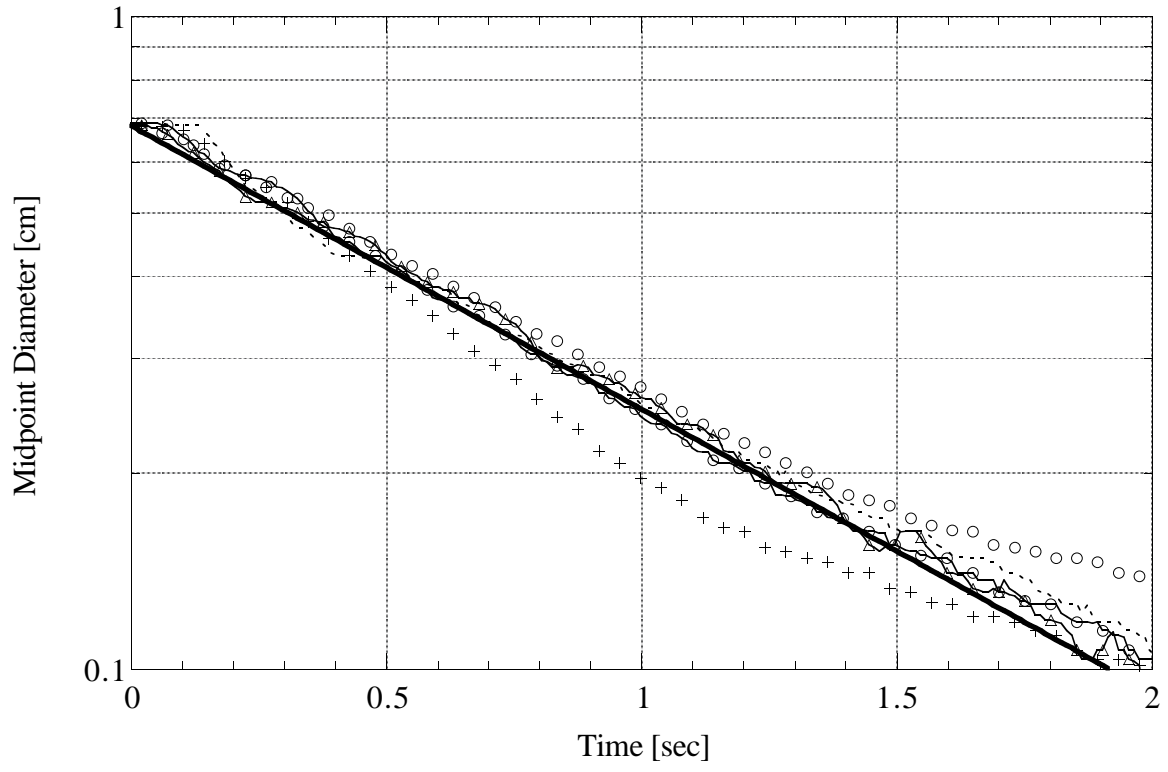


Figure 7

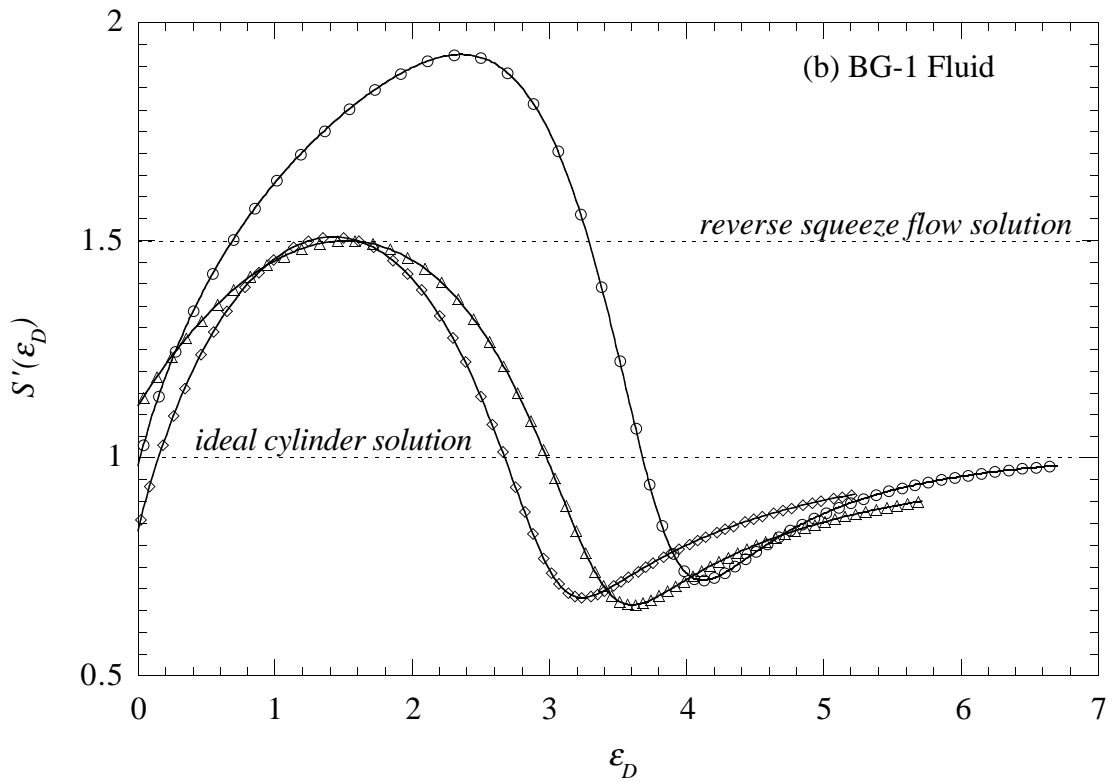
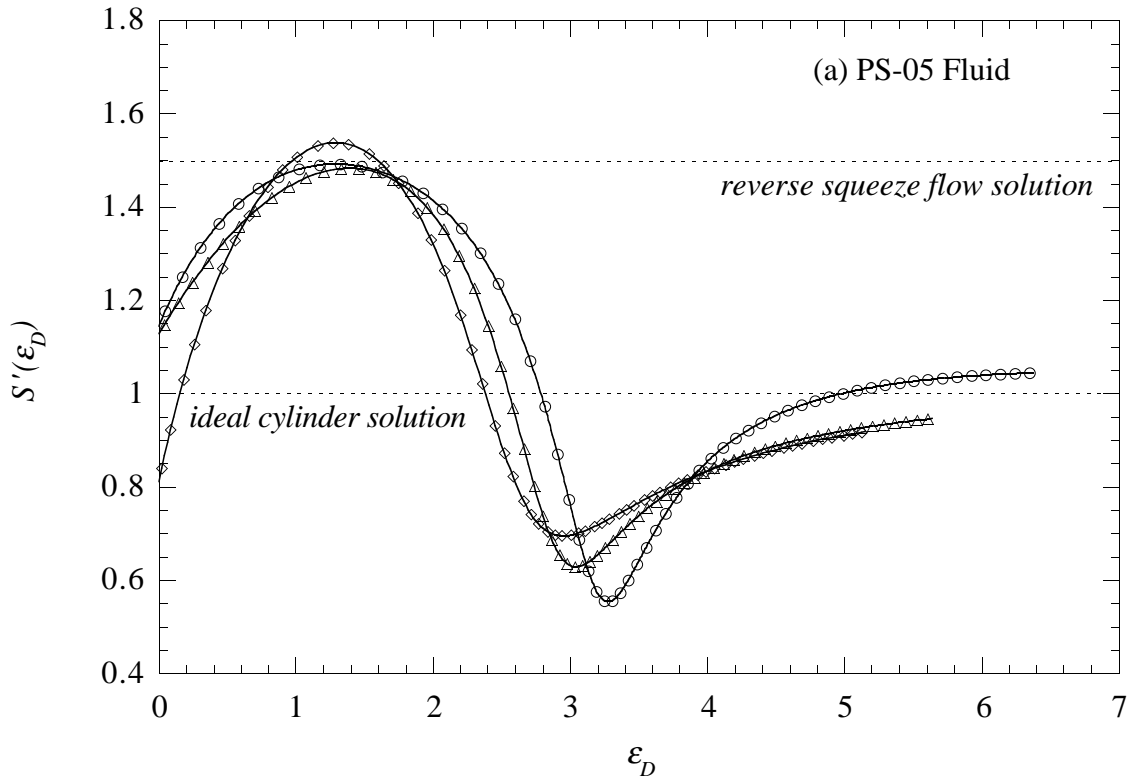


Figure 8

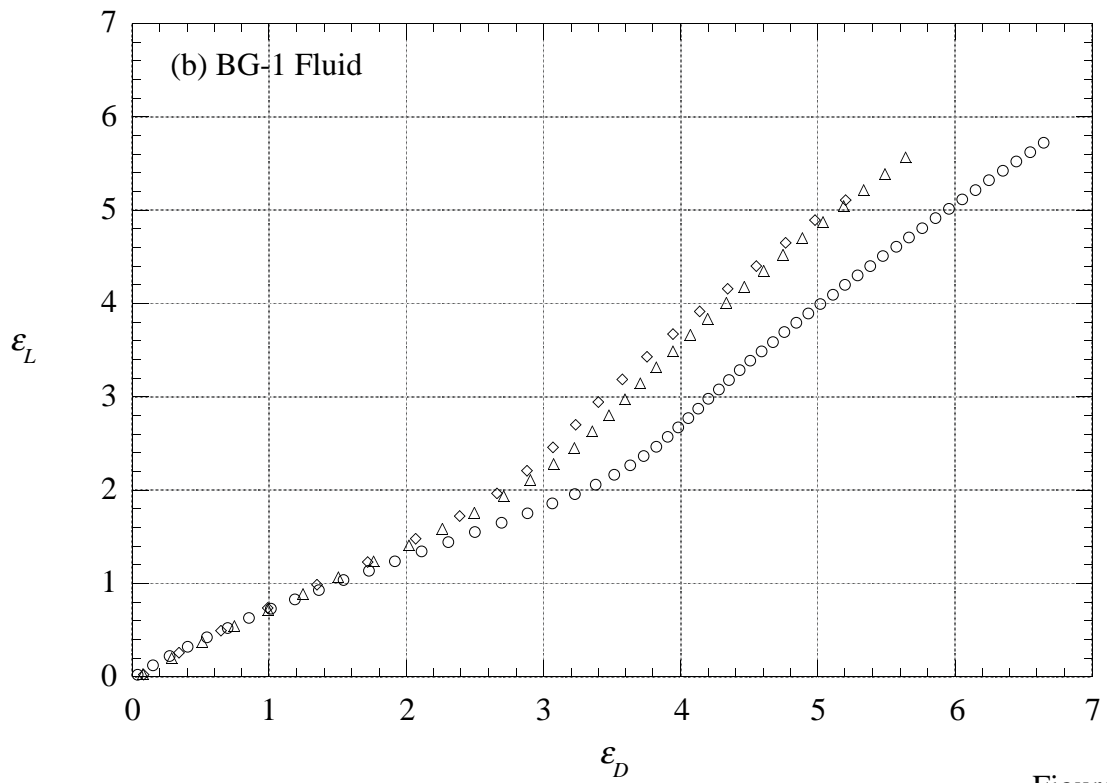
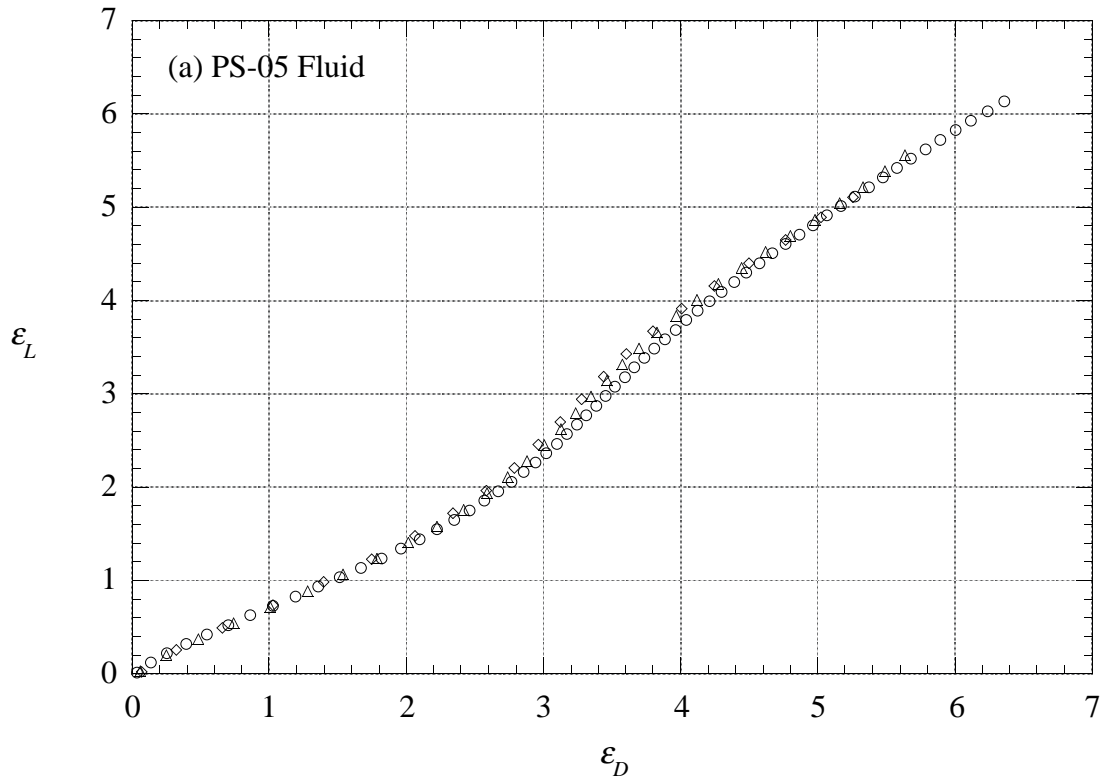


Figure 9

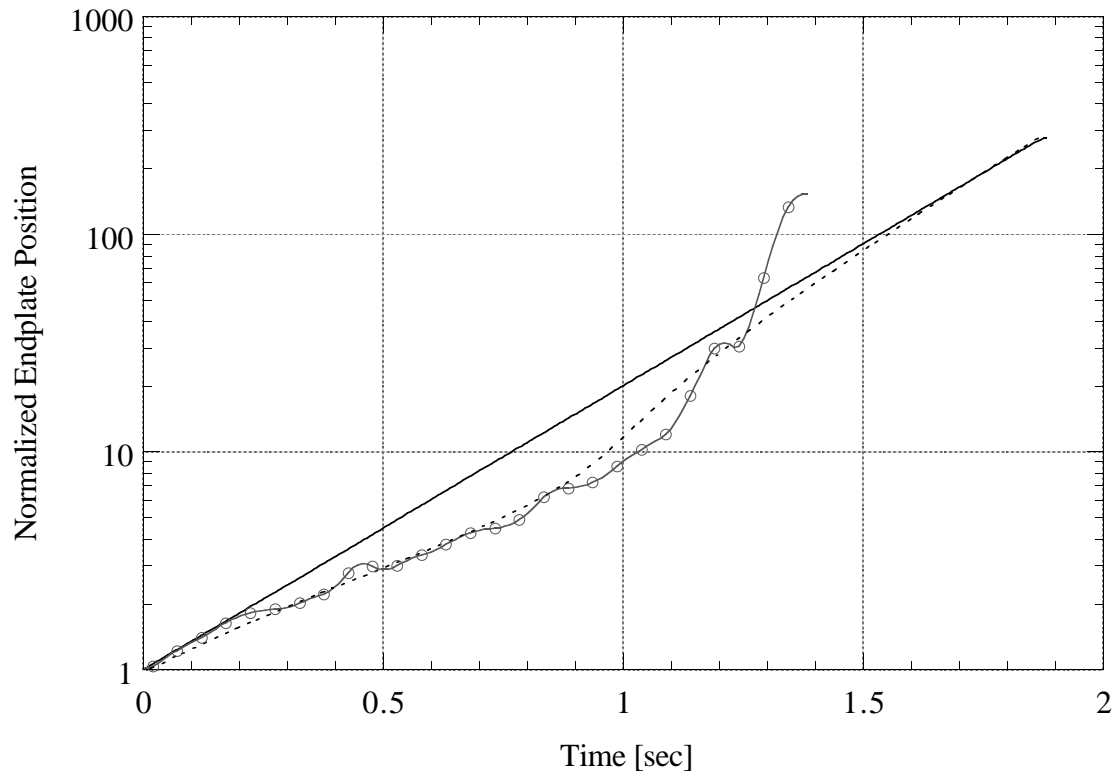


Figure 10

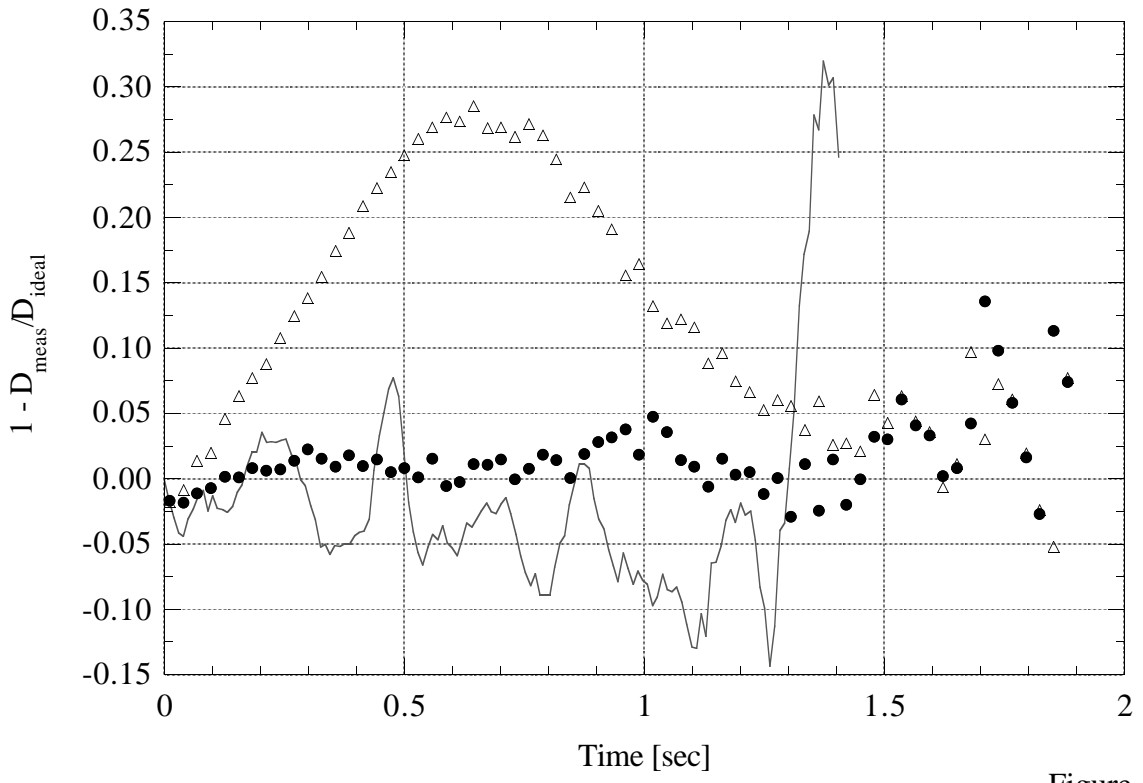
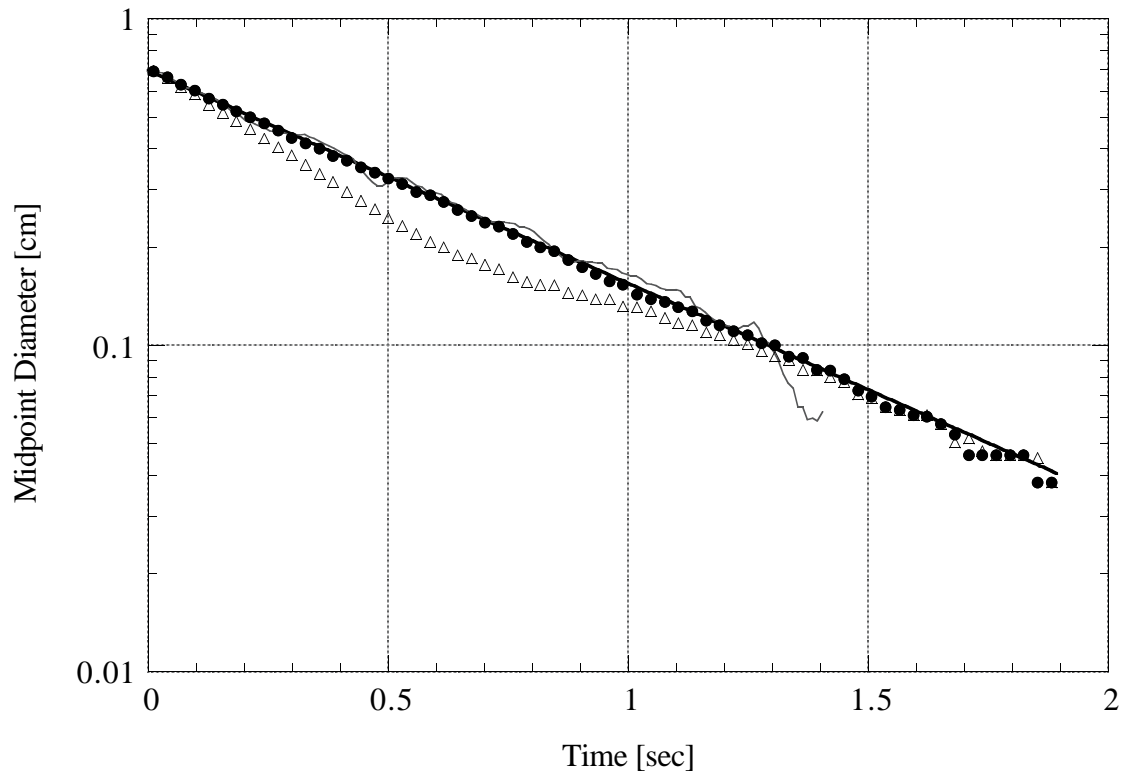


Figure 11

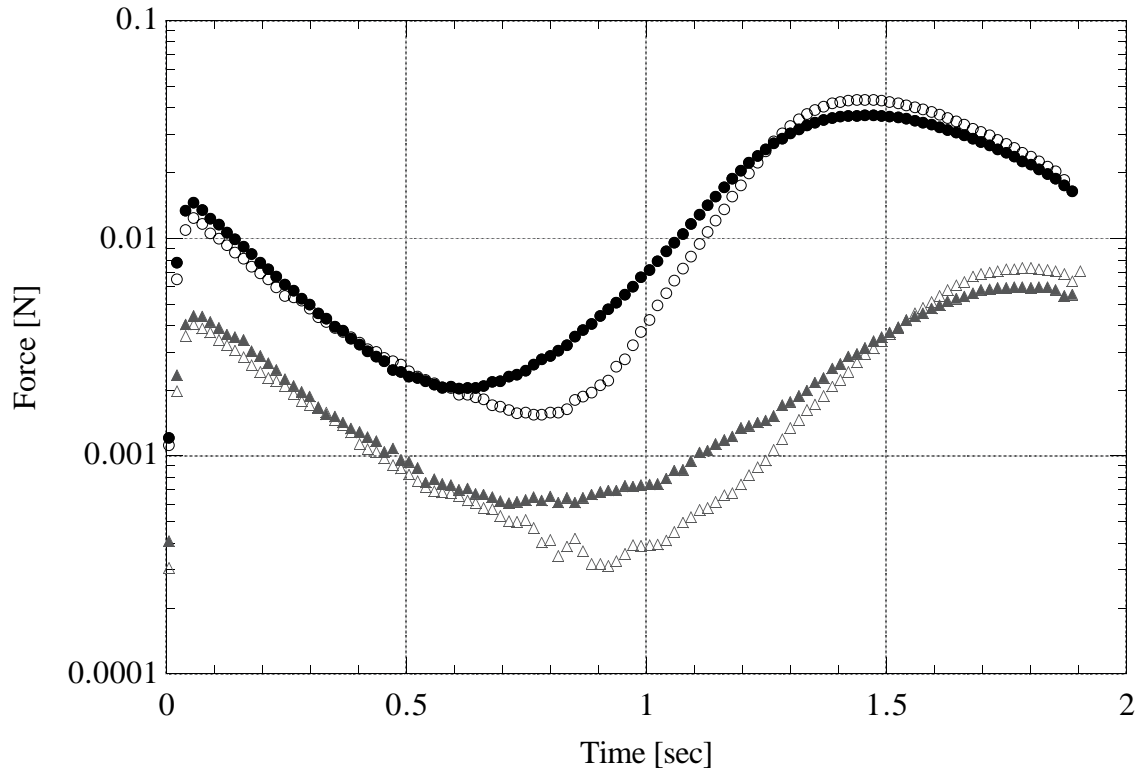


Figure 12

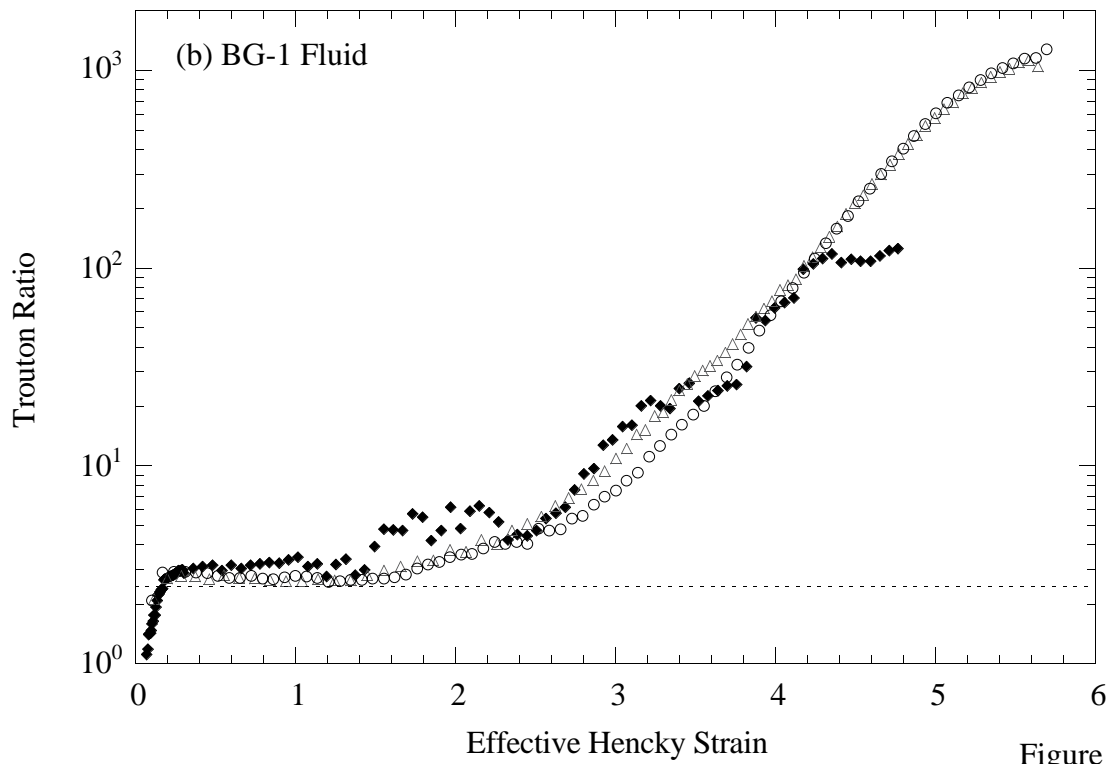
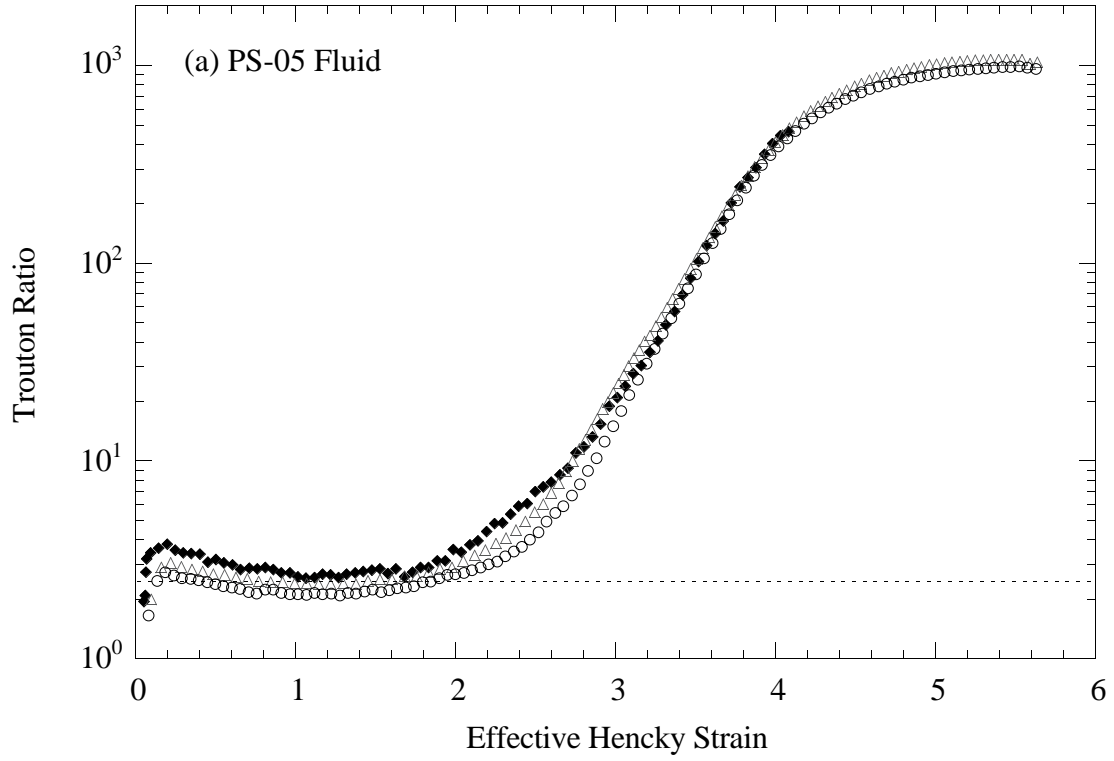


Figure 13

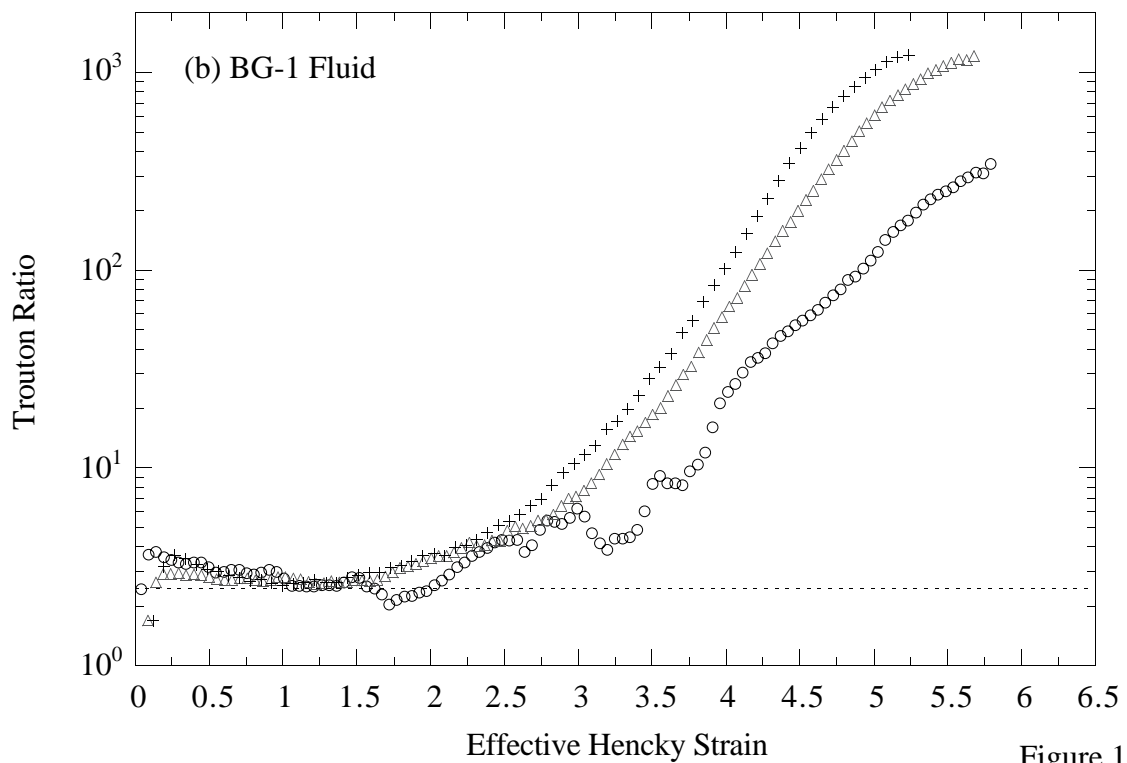
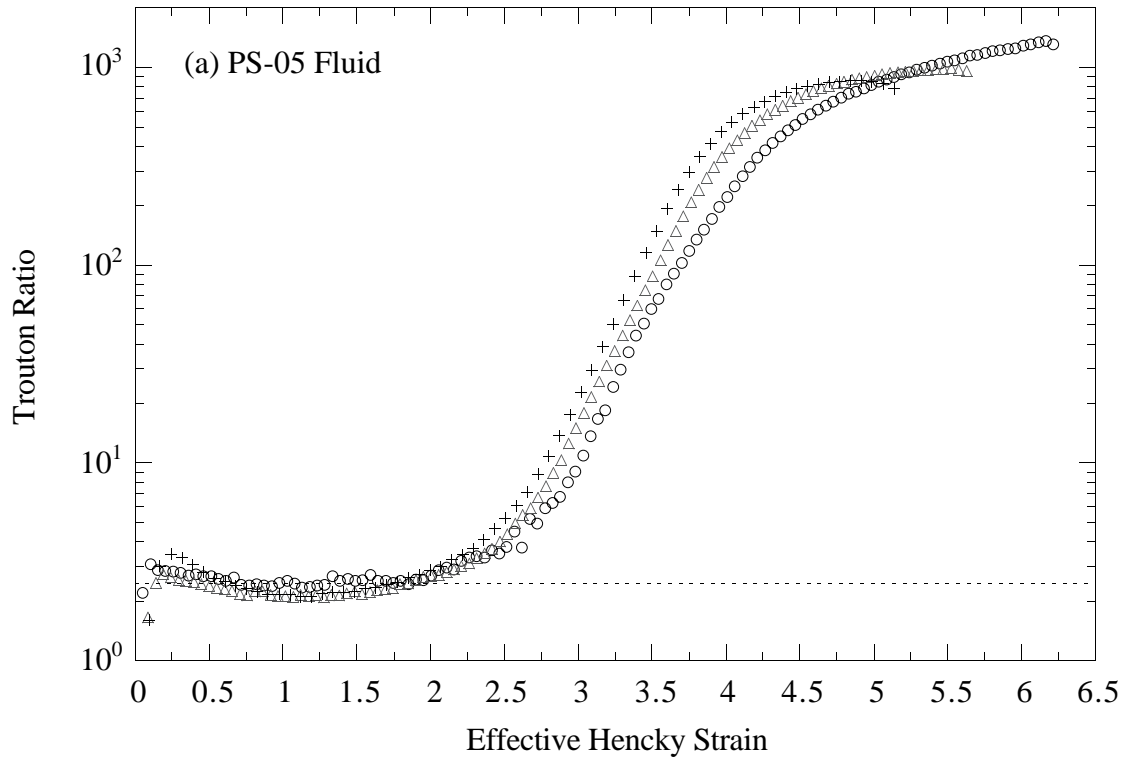


Figure 14

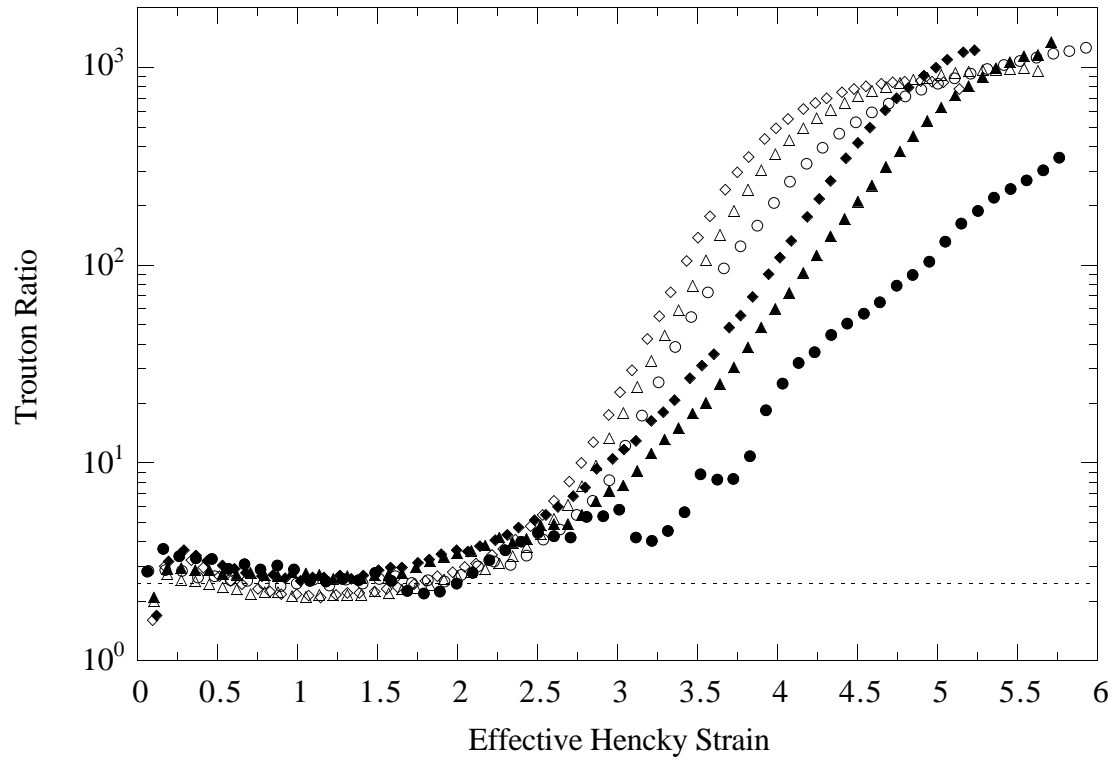


Figure 15